Pericyte-specific vascular expression of SARS-CoV-2 receptor ACE2 – implications for microvascular inflammation and hypercoagulopathy in COVID-19 patients

Liqun He[1*], Maarja Andaloussi Mäe[1*], Ying Sun[1], Lars Muhl[2], Khayrun Nahar[1], Elisa Vázquez Liébanas[1], Malin Jonsson Fagerlund[3] Anders Oldner[3], Jianping Liu[2], Guillem Genové[2], Riikka Pietilä[1], Lei Zhang[4], Yuan Xie[4], Stefanos Leptidis[2], Guiseppe Mocci[2], Simon Stritt[1], Ahmed Osman[5], Andrey Anisimov[6], Karthik Amudhala Hemanthakumar[6], Markus Räsenen[6], Johan Björkegren[2,7,8,9], Michael Vanlandewijck[2], Klas Blomgren[5,10], Emil Hansson[2], Taija Mäkinen[1], Xiao-Rong Peng[11], Thomas D. Arnold[12], Kari Alitalo[6], Lars I Eriksson[3], Urban Lendahl[2,13], Christer Betsholtz[1,2,14,§]

[*]Shared contribution

[§]Correspondence: christer.betsholtz@ki.se or christer.betsholtz@igp.uu.se

[1] Department of Immunology, Genetics and Pathology, Uppsala University, Uppsala, Sweden

[2] Integrated Cardio Metabolic Center (ICMC), Karolinska Institutet, Huddinge, Sweden

[3]Department of Physiology and Pharmacology, Section for Anesthesiology and Intensive Care Medicine, Karolinska Institutet, Solna and Function Perioperative Medicine and Intensive Care, Karolinska University Hospital, Stockholm, Sweden

[4]Key Laboratory of Ministry of Education for Medicinal Plant Resource and Natural Pharmaceutical Chemistry, National Engineering Laboratory for Resource Developing of Endangered Chinese Crude Drugs in Northwest of China, College of Life Sciences, Shaanxi Normal University, Xi'an, China

[5]Department of Women's and Children's Health, Karolinska Institutet, Solna, Sweden

[6]Wihuri Research Institute and Translational Cancer Medicine Program, Biomedicum Helsinki, University of Helsinki, Finland.

[7]Institute of Genomics and Multiscale Biology, Department of Genetics and Genomic Sciences, Icahn School of Medicine at Mount Sinai, New York, NY, US

[8]Department of Pathophysiology, Institute of Biomedicine and Translational Medicine, University of Tartu, Tartu, Estonia

[9]Clinical Gene Networks AB, Stockholm, Sweden

Cardiovascular, Renal and Metabolism (CVRM), IMED Biotech Unit, AstraZeneca BioPharmaceuticals R&D, Gothenburg, Sweden

[11]Department of Pediatric oncology, Karolinska University Hospital, Stockholm, Sweden

[12]Department of Pediatrics, University of California San Francisco, USA

[13]Department of Cell and Molecular Biology, Karolinska Institutet, Sweden

[14]Department of Medicine Huddinge, Karolinska Institutet, Sweden

Abstract

Accumulating clinical observations suggest pathogenesis beyond viral pneumonia and its secondary consequences in COVID-19 patients. In particular, many patients develop profound hyperinflammation and hypercoagulopathy with disseminated thrombogenesis and thromboembolism, which we observe also in a Swedish COVID-19 intensive care patient cohort. To understand these vascular manifestations, it is important to establish the potential vascular entry point(s) of the SARS-CoV-2 virus, i.e. which vascular cell types express the SARS-CoV-2 receptor ACE2. We present data that ACE2 is specifically and highly expressed in microvascular pericytes, but absent from endothelial cells, perivascular macrophages and fibroblasts. Mice with pericyte ablation show increased expression and release of Von Willebrand Factor from microvascular endothelial cells, suggesting that pericytes orchestrate thrombogenic responses in neighboring endothelial cells. Identifying pericytes rather than endothelial cells as the ACE2-expressing cells in the vasculature may explain why hypertension, diabetes and obesity are risk factors for severe COVID-19 patients, as these conditions are characterized by an impaired endothelial barrier function, allowing SARS-CoV-2 to reach and infect the pericytes that are normally shielded from the blood behind an intact endothelial barrier. This novel COVID-19-

pericyte hypothesis is testable, offers explanations for some of the most enigmatic and lethal aspects of COVID-19 and calls for further investigations into the possible benefits of preventive anticoagulant therapy.

Introduction

COVID-19 is a pandemic with currently more than 4.0 million confirmed cases and more than 280,000 deaths (As of May 11; Johns Hopkins University COVID-19 case tracker https://coronavirus.jhu.edu). COVID-19 is caused by the severe acute respiratory syndrome coronavirus-2 (SARS-CoV-2). Like other coronaviruses (Fehr and Perlman, 2015), SARS-CoV-2 infects cells through binding of its spike (S) protein to cell surface receptors, followed by S protein cleavage, fusion of viral and cellular membranes and viral RNA entry into the cytoplasm. Recently, angiotensin-converting enzyme 2 (ACE2) was identified as the cell surface receptor for SARS-CoV-2 and the cellular proteases TMPRSS2 and cathepsin B/L (CTSB/L) as mediators of SARS-CoV-2 S cleavage (Hoffmann et al., 2020). SARS-CoV-2 thereby appears to utilize the same molecular pathway for cellular entry as SARS–CoV-1, the causative coronavirus for the SARS epidemic in 2002-2003 (Li et al., 2005; Matsuyama et al., 2010). ACE2 normally functions in the renin/angiotensin pathway by cleaving angiotensin-2 to angiotensin 1-7, a peptide with multiple reported functions (Lovren et al., 2008; Ohishi et al., 2013). SARS-CoV-2 is a member of a larger family of coronaviruses, which includes other strains that infect humans, such as SARS-CoV, MERS-CoV and hCoV-229E. The SARS and MERS epidemics had high mortality rates, but dropped off before reaching pandemic levels. HCoV-229E causes mild upper airway infections (Fehr and Perlman, 2015; Navas-Martin and Weiss, 2004).

The vast majority of COVID-19 symptom carriers experience initial respiratory symptoms, indicating that the respiratory epithelium is the most common entry point for viral infection. Several subsets of surface epithelial cells in the nasal passage, lung, gastrointestinal tract and eye were recently shown to express combinations of ACE2/TMPRSS2 or ACE2/CTSL indicating susceptibility for SARS-CoV-2 infection (Muus et al., 2020; Sungnak et al., 2020; Ziegler et al., 2020). ACE2

expression on surface epithelial cells offers an explanation for the earliest range of COVID-19 symptoms, including cough, fever, respiratory disorder, lost sense of smell and taste, nausea and diarrhea. However, later during the disease course, COVID-19 patients sufficiently ill to become hospitalized also experience a range of other symptoms without an obvious link to the primary respiratory epithelial infection sites. This second wave of symptoms, which are prevalent particularly in the critically ill patients admitted to intensive care, includes coagulation abnormalities with subsequent thrombosis, thromboembolism and consequences thereof (pulmonary embolism, myocardial infarction and stroke), acute kidney injury and neurological symptoms (Batlle et al., 2020; Diao and al., 2020; Helms et al., 2020; Klok et al., 2020; Mao et al., 2020; Tang et al., 2020; Yang et al., 2020). Laboratory blood tests reveal hypercoagulation (Panigada et al., 2020; Spiezia et al., 2020) and systemic inflammation (Lazzerini et al., 2020; Quartuccio et al., 2020). The basis of the vasculature-associated manifestations of COVID-19 is, however, still poorly understood. While they may be considered as possible consequences of secondary bacteremia, they may also be a result of direct infection of the vasculature by SARS-CoV-2, particularly considering that the surface area of the vasculature is considerably larger than that of the lungs (Jaffe, 1987). Intriguingly, there is an increasing notion that some COVID-19 patients display severe hypoxemia without concomitant respiratory dysfunction early in the disease course (Leisman et al., 2020), posing the question of a possible vascular pathogenesis independent of pulmonary function. It is therefore important to ask which vascular cell types can serve as entry point(s) for SARS-CoV-2 infection of the vasculature, i.e. which vascular cells express ACE2, TMPRSS2 and CTSL/B.

The inner vascular lining consists of endothelial cells, which in most parts of the vasculature are connected to each other by junctional complexes, thereby forming a tight barrier. In the absence of inflammation, this barrier is not passively permeable to cells or macromolecules; instead endothelial cells utilize receptor-mediated transport mechanisms for extravasation of these moieties. Mural cells (pericytes and vascular smooth muscle cells (VSMCs)) reside immediately outside of the endothelial tubing and are embedded within the same basement membrane as the

endothelium. They provide mechanical support and regulate vascular tone, while fibroblasts and macrophages constitute other distinct types of perivascular cells. In large parts of a non-injured vasculature, the blood is in direct contact only with the endothelial cells, but in a number of pathological conditions, such as hypertension, diabetes and obesity, the integrity of the endothelial barrier is compromised (Chistiakov et al., 2015; Madonna et al., 2017; Mundi et al., 2018; van Sloten et al., 2020; Yuan et al., 2007). Interestingly, these conditions are also recognized as the most common co-morbidities for hospitalized COVID-19 patients (Fang et al., 2020; Richardson et al., 2020).

Thus, there is considerable interest in establishing which vascular cell types express ACE2 and its associated proteases, but the available data are as yet somewhat conflicting. Our previous work, including bulk and single-cell RNA sequencing (scRNAseq), identified *Ace2* as one of a relatively limited number of mRNA markers for pericytes in mouse brain vasculature (He et al., 2018; He et al., 2016; Vanlandewijck et al., 2018), and a recent single-nucleus (sn)RNAseq study of the human heart also pinpointed pericytes as putative sites of ACE2 expression (Chen et al., 2020a). In contrast, other studies, based on cell culture and immunostaining of tissue sections, have suggested ACE2 expression in vascular endothelial cells (Lovren et al., 2008; Sluimer et al., 2008). Furthermore, a recent scRNAseq meta-analysis from the Human Cell Atlas consortium reports *ACE2* expression in pericytes as well as in endothelial cells, fibroblasts and macrophages from multiple organs (Muus et al., 2020). To precisely define which vascular cell types express ACE2 is not only of academic interest, but has direct medical relevance, as endothelial cells are exposed to blood-borne SARS-CoV-2 both in healthy and diseased states, while cell types located outside of the endothelial barrier, such as pericytes, would only be expected to face the virus in an abnormally permeable vasculature.

To address the vascular localization of ACE2, we undertook a focused analysis of the expression of ACE2, TMPRSS2 and CTSB/L in mouse and human vascular cells. We demonstrate that ACE2 is specifically expressed in pericytes and venous VSMCs, but importantly, it is not expressed in endothelial cells, arterial VSMCs, macrophages or

fibroblasts, at least not in the organs assessed herein. Given the pericyte specificity of ACE2 expression, we analyzed mouse models of pericyte loss in order to gain insights into the role of pericytes in vascular dysfunction relevant for COVID-19-associated coagulopathy. Loss of pericytes induced a marked upregulation and secretion of Von Willebrand Factor in microvascular endothelial cells, as well as platelet aggregation and fibrin deposition, all hallmarks of disturbed thrombogenic homeostasis. Based on a combination of clinical, transcriptomic and mouse model data, we hypothesize that SARS-CoV-2 infection of pericytes is causative for the increased thrombogenicity and hypercoagulation observed in COVID-19 patients. Moreover, our hypothesis implies that in order to reach the pericytes, the virus has to pass through a dysfunctional endothelial barrier.

Results

Thrombosis, thromboembolism, hypercoagulation and systemic inflammation in COVID-19 patients in intensive care in the Stockholm region

It is an emerging view that vasculature-associated pathologies are observed in COVID-19 patients (Bikdeli et al., 2020; Cattaneo et al., 2020; Helms et al., 2020; Le Berre et al., 2020; Poissy et al., 2020; Sardu et al., 2020; Zhou et al., 2020). To explore the extent and nature of such pathologies in a Swedish patient cohort, we studied clinical characteristics, systemic inflammation and coagulation abnormalities in 20 critically ill patients admitted to the intensive care unit at the Karolinska University Hospital, Stockholm, Sweden with positive diagnostic test for COVID-19 (for details see Table 1). The ICU patients had a median age of 63 years (range 40-73), the majority being male (90%) and having one or more risk factors prior to admission (85%). The length of ICU stay and duration of invasive mechanical ventilation reveal the severity of disease and treatment challenge. Furthermore, most of them required mechanical ventilation in prone position due to critical hypoxia with periods of high inspired fractions of oxygen (FiO_2) and a low arterial oxygen tension to FiO_2 ratio index (PFI). These patients uniformly showed a systemic hyperinflammatory state including markedly elevated C-reactive protein (CRP), high circulating levels of pro-inflammatory cytokines (e.g. IL-6) combined with profound

coagulation abnormalities, including high D-dimer and high levels of fibrinogen. Even more important, 30% of this cohort had confirmed pulmonary embolism despite prophylactic anticoagulation therapy.

Ace2/ACE2 is specifically expressed in microvascular mural cells in the brain

The observed severe systemic inflammation and advanced coagulopathy in the COVID-19 patients in intensive care prompted us to ask where the vascular entry point(s) for SARS-CoV-2 infection may reside, and we therefore analyzed the expression of receptors for SARS-CoV-2, i.e. ACE2 and S priming proteases by vascular cells. Mice and humans frequently share gene and protein expression patterns across cell types, and although mice are not productively infected by SARS-CoV-2 (Cohen, 2020; Monteil et al., 2020) (likely because mouse ACE2 does not recognize the SARS-CoV-2 S-protein), we first assessed ACE2 distribution in the mouse brain vasculature.

We have previously reported that *Ace2* mRNA is enriched in vascular mural cells in the mouse brain (He et al., 2016), and our subsequent scRNASeq analysis of the brain vasculature showed that *Ace2* is one of the top 15 markers for pericyte and venous VSMCs. (He et al., 2018; Vanlandewijck et al., 2018) (http://betsholtzlab.org/VascularSingleCells/database.html). When re-assessing these data, we noted that in addition to pericytes and venous VSMCs, *Ace2* is also expressed by arteriolar and some arterial VSMCs, albeit at lower levels than in pericytes and venous VSMCs (Fig 1A). The *Ace2*-positive arterial VSMCs formed a subgroup of *Cnn1*-negative cells (Fig 1B) present in small arterioles (Vanlandewijck et al., 2018). The *Ace2*-negative *Cnn1*-positive VSMCs expressed a unique set of other markers for VSMCs present in larger arterioles and arteries (Suppl Fig 1A). In addition, we found a small population of *Ace2*-positive cells among the brain type-2 fibroblasts (FB2) and a small number of *Ace2*-positive endothelial cells distributed in different endothelial clusters (Fig 1B). In both these cases, the *Ace2*-positive cells co-expressed the pericyte marker *Kcnj8* (Fig 1B), as well as several other pericyte markers (Suppl Fig 1B, C). However, they lacked a distinctive transcript pattern beyond pericyte markers on top of the FB2 and endothelial transcriptomes, respectively, suggesting that they were pericyte-contaminated (Suppl Fig 1B, C).

Deep analysis of the 23 *Ace2*-positive endothelial cells in the SmartSeq2 dataset revealed that 20 of them expressed at least one additional pericyte marker, and 18 of them expressed multiple pericyte markers (Fig 1C, top), whereas pericyte markers were absent from most *Ace2*-negative endothelial cells (Fig 1C, bottom). The top 50 enriched genes in the three *Ace2*-positive endothelial cells lacking other tested pericyte markers did not reveal a statistically significant gene profile, suggesting that they do not represent a rare endothelial subtype (Suppl Fig 1D).

To deepen our analysis of the vascular cells, we devised a computational pipeline for scRNAseq meta-analysis of SmartSeq2 and 10x (DropSeq) data (see Materials and Methods). We used this pipeline to merge the data set analyzed above (He et al., 2018) with another SmartSeq2 data set (Tabula Muris et al., 2018) and an unpublished dataset generated using the 10x (DropSeq) platform (Suppl Fig 1E). Meta-analysis of these three datasets confirmed specific *Ace2* expression in pericytes, venous VSMCs and *Cnn1*-negative arteriolar VSMCs (Suppl Fig 1F, G). An additional *Ace2*-positive cell cluster in the 10x dataset (#17 in Suppl Fig 1G) contained both pericyte and endothelial markers, but lacked other unique transcripts, indicating that it was composed of endothelial cell-pericyte doublets.

Next, we assessed the localization of ACE2-expressing cells in mouse brain vasculature by immunofluorescent staining (IF) for ACE2 along with specific markers for mural cells and endothelial cells. Focusing on the brain cortex, where vascular arterio-venous identities can readily be identified through morphology and marker expression, we found ACE2-positive cells fitting the expected location and marker expression of pericytes and microvascular VSMCs (Fig 1D and Suppl Fig 2). No ACE2 IF signal was detected in any other cell types in this part of the brain.

To extend the analysis of *Ace2* expression to non-vascular cell types in several regions of the brain, we explored the mousebrain.org atlas, and this analysis confirmed that *Ace2* is not expressed appreciably outside of the vasculature across 265 different central and peripheral nervous system cell types (Zeisel et al., 2018) (http://mousebrain.org/genesearch.html). More specifically, analysis of the mousebrain.org database revealed *Ace2* expression mainly in pericytes, but also in a cluster of endothelial cells, which however co-expressed numerous pericyte markers (including *Pdgfrb* and *Notch3*) indicating their mural cell contamination.

To analyze *ACE2* expression in mural cells of the human brain is currently difficult, given the scarcity of scRNAseq data for these cells, presumably because it is difficult to capture mural cells for scRNAseq or snRNAseq analysis. In a dataset representing the developing human prefrontal cortex (Zhong et al., 2018), we however identified six *ACE2*-positive cells expressing at least one pericyte marker, and three of them expressed multiple pericyte markers (Fig 1E). We also assessed a human glioblastoma drop-seq 10x scRNAseq dataset consisting of 69,125 endothelial and immune cells sorted using anti-CD31 antibodies (Zhang et al, unpublished). Among these, we found two *ACE2*-positive cells, which had pericyte markers, but lacked high abundance brain endothelial markers (Fig 1F). In summary, our data indicate that human brain pericytes express *ACE2.*

Collectively, these analyses show that among the more than 200 cell types estimated to make up the mouse brain, only pericytes, venous VSMCs and small arteriolar VSMCs express *Ace2*. Importantly, we found no convincing scRNAseq evidence for *Ace2* expression in endothelial cells in the brain, thus previous annotations of *Ace2*-positive cells in the brain as endothelial cells are most likely due to pericyte contamination.

ACE2 is specifically expressed in pericytes of the heart

We next analyzed *Ace2/ACE2* expression in mouse and human heart. Recent results deposited by the Human Cell Atlas consortium suggest that *ACE2* is expressed by cardiac pericytes, but *ACE2* expression was additionally reported in cardiomyocytes, endothelial cells and fibroblasts (Muus et al., 2020). When analyzing our mouse heart scRNAseq data on fibroblasts and mural cells obtained by fluorescence-activated cell sorting from *Pdgfrb*-GFP transgenic mice, we found prominent expression of *Ace2* in pericytes but undetectable expression in other cell types (data not shown). To more comprehensively analyze the expression of *Ace2* in the heart and to include additional cardiac cell types in the analysis, we used our meta-analysis pipeline to integrate three unpublished and one published datasets (Tabula Muris et al., 2018). These combined data provide comprehensive coverage of the principal cell types in the heart, including cardiomyocytes, different types of endothelial cells (blood vascular, endocardial, lymphatic), different types of mural cells (pericytes,

VSMCs), and different subtypes of fibroblasts and macrophages (Fig 2A). Of these, only pericytes expressed *Ace2* substantially (Fig 2B, C). As in the brain, only few endothelial cells displayed RNAseq counts for *Ace2*. Of 21 *Ace2*-positive heart endothelial cells (Suppl Fig 3A), 18 expressed at least one pericyte marker and 15 expressed multiple pericyte markers (Suppl Fig 3B). Pericyte marker expression was also found in some *Ace2*-negative endothelial cells, but at lower frequency and level (Suppl Fig 3B). Analysis of the three *Ace2*-positive cells without expression of other assessed pericyte markers did not reveal any indications of a common cell subtype or state (Suppl Fig 3C). Therefore, we conclude that the *Ace2*-positive endothelial cells found in the mouse heart were pericyte-contaminated.

We next analyzed cardiac ACE2 expression by IF in tissue sections from adult mouse heart. This revealed ACE2 IF signal only in cells with a microvascular location typical for pericytes (Fig 2D and Suppl Fig 4). In the *Pdgfrb*-GFP reporter mouse, ACE2 IF overlapped with GFP expression, which, due to its high fluorescence intensity, verified that ACE2 IF positive cells had the typical morphology of pericytes, with a distinct cell body and long slender processes extending along the CD31-positive endothelial cells (Fig 2D). When compared to the brain, an interesting difference in the heart was that *Ace2* mRNA and protein were located exclusively in pericytes, whereas the mural cells of veins and small coronary arterial branches were negative (Fig 2C, D and Suppl Fig 4). Another difference to the brain was that not all *Pdgfrb*-GFP pericytes were ACE2 positive: the relative ACE2/*Pdgfrb*-GFP signal varied extensively between cells (cells #1 and #2 in Fig 2D, bottom panel) and some strongly *Pdgfrb*-GFP pericytes appeared ACE2-negative (cell #3 in Fig 2D, bottom panel). The subcellular distribution between *Pdgfrb*-GFP and ACE2 was also different, as expected for proteins with cytoplasmic (GFP) and cell membrane (ACE2) locations: GFP provided strong labeling of the cell soma, whereas ACE2 provided a relatively stronger labeling of the pericyte processes (Fig 2D and Suppl Fig 3).

In order to assess *ACE2* expression in the human heart, we downloaded and re-analyzed a published scRNAseq dataset generated from healthy adult human hearts (Wang et al., 2020a) (Fig 3A). We identified a cluster of cells with substantially higher *ACE2* expression than the other clusters (Fig 3B). We annotated cell type identities based on canonical markers and inference of gene expression patterns in

mouse cardiac cells, where pericytes, VSMCs and fibroblasts have been unambiguously identified by a combination of scRNAseq and tissue analysis (Muhl et al, submitted). This analysis defined the human *ACE2*-high cluster as pericytes (Fig 3B). In addition, a cluster annotated as fibroblasts contained a minor proportion of *ACE2*-positive cells (cluster 7 in Fig 3B), and given the paucity of specific markers distinguishing pericytes from fibroblasts in the human heart, we could not establish whether the data reflect true fibroblast expression of *ACE2* or fibroblast-pericyte contamination. One of the endothelial clusters also contained a few *ACE2*-positive cells (cluster 2 in Fig 3B), which, however, had also pericyte markers (Fig 3C). Some of the *ACE2*-negative endothelial cells were also pericyte marker positive. As in the mouse, they occurred at lower frequency and level than among the *ACE2*-positive endothelial cells (Fig 3C). We therefore concluded that the *ACE2*-positive human cardiac endothelial cells were pericyte-contaminated. All other cardiac cells, including cardiomyocytes, endothelial cells, endocardial cells and macrophages were *ACE2*-negative. Collectively, our analyses of mouse and human healthy adult heart scRNAseq data establish pericytes as the major, perhaps sole, cellular source of *Ace2/ACE2* in the adult heart.

In the lung, airway epithelial cells form the major *Ace2/ACE2* expression site

The lungs are a primary target of SARS-CoV-2 infection. Our scRNAseq dataset of pulmonary vascular cells (Vanlandewijck et al., 2018) did not reveal appreciable *Ace2* expression in lung endothelial cells or pericytes. Instead, we found a distinct *Ace2* signal in a cluster of epithelial cells that coexpressed markers of multiciliated epithelium (He et al., 2018; Vanlandewijck et al., 2018). To obtain a deeper insight into *Ace2* expression by different pulmonary cell types, we used our meta-analysis pipeline to integrate three published and two unpublished adult mouse lung scRNAseq datasets (Fig 4A). Exploring the *Ace2* mRNA distribution in the combined data revealed significant expression only in alveolar type-2 (AT-2) cells and multiciliated airway epithelial cells (Fig 4A, B). There was no *Ace2* expression in any of the subtypes of vascular endothelial cells, mural cells, fibroblasts, alveolar macrophages or other immune cells (Fig 4B). IF analysis of ACE2 protein in adult mouse lungs corroborated the scRNAseq analysis. A prominent ACE2 IF signal was

detected in bronchial epithelium and in a population of scattered alveolar cells corresponding to the location of AT-2 cells (arrows in Fig 4C). The alveolar ACE2 staining did not overlap with markers of endothelium (CD31) or pericytes (CSPG4), which was in agreement with the lack of *Ace2* mRNA in these cell types (Fig 4C and Suppl Fig 5).

In order to explore *ACE2* expression in human lungs, we re-analyzed scRNAseq data from the lungs of adult human transplant donors and lung fibrosis patients (Reyfman et al., 2019). In these, AT-2 cells constituted the major cellular source of *ACE2* transcripts, but expression could be detected also in basal, club and multiciliated cells (Suppl Fig 6). Immune cells, endothelial cells and fibroblasts were *ACE2* negative, but the vascular cell sample size was too small for a comprehensive analysis. Mural cells, for example, were not present in the dataset.

We also analyzed the expression of the SARS-CoV-2 S protein priming proteases. We observed a high level of *Ace2* co-expression with *Tmprss2* in epithelial cells across the mouse lung dataset, whereas *Ctsl* and *Ctsb* were more broadly expressed (albeit weakly in hematopoietic cells) (Suppl Fig 7). However, *Tpmrss2* was not expressed in pericytes, which instead exhibited co-expression of *Ace2* with *Ctsb* and *Ctsl* in the brain and heart (Suppl Fig 7).

Taken together, our observations confirm recent reports (Muus et al., 2020; Sungnak et al., 2020) in pinpointing AT-2 cells and other epithelial cells as the primary sites of *ACE2* mRNA and protein expression in the lung. Furthermore, our data reveal differences in the S protein priming proteases that are expressed in pulmonary epithelial cells (TMPRSS2) and pericytes (CTSB/L) in the brain and heart.

Pericyte hypoplasia elicits an endothelial pro-coagulant response

The transcriptomic data from heart and brain identified pericytes as the predominant *Ace2*-expressing cells in these organs. Given the roles of pericytes in vascular barrier formation and in restraining pro-inflammatory responses in endothelial cells (Armulik et al., 2010; Daneman et al., 2010; Hong et al., 2015; Török et al., 2019) (Mäe et al, submitted), we analyzed pro-thrombotic responses in adult mice with constitutive hypoplasia of pericytes caused by decreased PDGF-B signaling via PDGFR-β receptors (*Pdgfb*$^{ret/ret}$ mice) (Lindblom et al., 2003). In addition to

pericyte loss and development of dilated capillaries, we found more Von Willebrand Factor (*Vwf*) mRNA and protein (VWF) in the *Pdgfb*$^{ret/ret}$ mice than in *Pdgfb*$^{ret/+}$ littermate control mice, which had normal microvascular pericyte coverage (Fig 5A, B). VWF promotes platelet adhesion and blood coagulation in wounds through binding and stabilization of factor VIII. In controls, VWF mRNA and protein were mainly confined to arterioles and venules with limited or undetectable presence in capillaries, whereas the dilated capillaries that show signs of pro-inflammatory activation in *Pdgfb*$^{ret/ret}$ mice (Armulik et al., 2010) (Mäe et al, submitted) were strongly and uniformly VWF-positive (Fig 5A, B). The VWF IF signal was primarily localized to intracellular rod-shaped vesicles (Weibel-Palade bodies) (Suppl Fig 8 and Suppl video 1), but it was also frequently observed as a "halo" around vessels in the *Pdgfb*$^{ret/ret}$ brain parenchyma, presumably due to local VWF release (Fig 5B,C, see also Fig 6B). We next assessed platelet adherence and aggregation in the *Pdgfb*$^{ret/ret}$ vessels by analyzing CD41 IF and fibrinogen (FBG) leakage and fibrin deposition (Fig 6A). Sites displaying both platelet aggregation and fibrin deposition were commonly observed in brain sections from *Pdgfb*$^{ret/ret}$ mice (Fig 6A), whereas in controls, we only observed a few individual adhered platelets, but no signs of platelet aggregation or FBG/fibrin deposition (data not shown). We also found that VWF release into the interstitium coincided with 70 kDa dextran tracer leakage into the brain parenchyma, demonstrating a local impairment of the blood-brain barrier at these sites (Fig 6B). In summary, these data reveal an important role for pericytes in restricting pro-coagulant responses in endothelial cells.

Discussion

The "COVID-19-pericyte hypothesis"

Our studies have led to the "COVID-19-pericyte hypothesis" shown in Fig 7. Specific ACE2 expression in pericytes and, in some organs, also in venous and arteriolar VSMCs, targets these vascular cell types to SARS-Cov-2 infection. Their location outside of the microvascular endothelial permeability barrier suggests that their infection occurs when the barrier is compromised and vessels become leaky, allowing the blood-borne virus to reach the pericytes. Infection of pericytes may

render them dysfunctional, leading to activation of pro-inflammatory and pro-thrombotic responses in the neighboring endothelial cells. Immune-attack (Perlman and Dandekar, 2005) of the infected pericytes should cause microvascular inflammation that exacerbates vascular leakage and endothelial pro-inflammatory and pro-thrombotic responses. Because of the increased vascular leakage more SARS-CoV-2 would extravasate from the blood, infect additional pericytes, and further intensify and propagate the microvascular inflammation and thrombosis. Below, we elaborate step-by-step the COVID-19-pericyte hypothesis and evidence supporting it, as well as the remaining gaps. Finally, we discuss implications of the hypothesis for the understanding of COVID-19 pathogenesis and therapy.

SARS-CoV-2 infects pericytes but not endothelial cells or other perivascular cell types

Accumulating data from analysis of single cell- or single-nucleus transcriptomes suggest that ACE2 is expressed by several epithelial subtypes in the lung, nasal cavity, cornea and conjunctiva and gastrointestinal (GI) tract (Muus et al., 2020; Sungnak et al., 2020; Ziegler et al., 2020), arguing that several of these surface epithelia serve as the primary entry point for the SARS-CoV-2 virus. Infection of various airway and GI-tract epithelial cells offers plausible explanations for many of the common symptoms of COVID-19 infection, such as cough, loss of smell, pneumonia and diarrhea. However, infection of these primary sites does not adequately explain the systemic inflammation and coagulopathy associated with COVID-19. We surmise that SARS-CoV-2 disseminates into the blood from the sites of primary infection. SARS-Cov-2 RNA can indeed be detected in blood (Wang et al., 2020b), and, importantly for the COVID-19-pericyte hypothesis, detection of SARS-Cov-2 RNA in blood has been reported to be a strong indicator of further clinical severity (Chen et al., 2020b).

A cornerstone of the COVID-19-pericyte hypothesis is that pericytes (along with venous and arteriolar VSMCs) are *the only* ACE2-positive cells in the vasculature. It has previously been reported that endothelial cells express ACE2 protein (Sluimer et al., 2008), but this study did not distinguish between ACE2 immunolabeling of endothelial cells versus pericytes. Recent scRNAseq studies also

report *ACE2* mRNA expression in cell clusters annotated as endothelial cells (Muus et al., 2020). In those cases where we were able to access the primary data, we consistently found evidence for pericyte contamination of the *ACE2*-expressing endothelial cells. We observe this also in rare *Ace2/ACE2* positive "endothelial" cells present in our own data. The mechanical and enzymatic separation of endothelial cells and pericytes poses particular challenges when tissues are dissociated for single-cell analysis, presumably because the two cell types firmly adhere to each other and their common basement membrane that is hard to fully digest without impairing cell viability (Vanlandewijck et al., 2018) (Muhl et al, submitted). Without optimized cell-dissociation protocols and positive-negative selection using cell-type specific markers, a variable proportion of heterotypic endothelial cell-pericyte doublets and cellular fragments will contaminate the sample.

In addition to the endothelial cells, we did not find any consistent expression of *Ace2/ACE2* in tissue macrophages or other hematopoietic cells, or in cardiomyocytes, which all have been reported to express *ACE2* (Muus et al., 2020; Tucker and al., 2020; Zou et al., 2020). We also found that a small subgroup of *Ace2*-positive fibroblasts in the brain were most likely pericyte-contaminated, and this may also be the case for the *ACE2*-positive fibroblasts reported by the Human Cell Atlas Consortium (Muus et al., 2020). Moreover, our data show that while pericytes in heart and brain express high levels of *Ace2/ACE2* mRNA, lung pericytes, and in addition, hepatic stellate cells and kidney mesangial cells, which are considered to be specialized pericytes, did not express *Ace2* (data not shown). Furthermore, venous and arteriolar VSMCs, which were positive for ACE2 mRNA and protein in the brain, were negative in the heart. Overall, we conclude that vascular *Ace2/ACE2* expression occurs primarily in *microvascular mural cells*, but also that the more precise microvascular expression patterns vary between different organs.

Do ACE2 positive pericytes become SARS-CoV-2 infected, and, if so, how? Pericytes reside within the microvascular basement membrane outside of the microvascular endothelium, and they are therefore normally not in direct contact with blood (Armulik et al., 2011). The virus particles would reach the pericytes if they could pass the endothelial barrier, which is formed by tight and adherens junctions connecting the endothelial cells. Passage through the endothelial layer occurs

through paracellular paths (when endothelial junctions are discontinuous), via transcellular routes, such as endothelial fenestrations, or by vesicular transcytosis (Claesson-Welsh, 2015). However, viral transport across the endothelial barrier appears unlikely considering the absence of ACE2 expression in endothelial cells. Given the reported diameter range of 70-150 nm for SARS-Cov-2 and SARS-Cov-1 (https://www.flickr.com/photos/niaid/albums/72157712914621487)(Kim et al., 2020; Neuman et al., 2006; Varga et al., 2020), it is unlikely that the virus is transported though endothelial pores, as the physiological upper limit of the pore size is ≈ 5-12 nm in most types of capillaries, including non-sinusoidal fenestrated blood capillaries with diaphragm-containing fenestrae (Sarin, 2010). For brain capillaries endowed with the blood-brain barrier, the upper pore size limit is less than one nm in physiological conditions. Although the diameter of individual fenestrae is comparable to that of the coronavirus particle, i.e. about 100 nm (Braet and Wisse, 2002), the physiological upper pore size limit of fenestrae without diaphragms is ≈ 15 nm in vessels in kidney glomeruli and ≈ 60 nm in bone marrow sinusoids, lymph nodes and liver (Aird, 2007; Sarin, 2010; Wisse et al., 2008). Furthermore, if the virus were able to pass through the endothelium, it would face a basement membrane with a pore size smaller than the diameter of the virus particle (Liliensiek et al., 2009). Even in one of the most permeable vascular beds known, the glomerular capillaries, it is hard to conceive viral passage, as the diameter of the podocyte filtration slits is ≈ 25 nm. For viral infection of renal proximal tubular epithelial cells, which express ACE2 (Lely et al., 2004), and for viral dissemination into urine (Peng et al., 2020), it is conceivable that the virus translocates through damaged vasculature either in glomerular or peritubular capillaries. In the context of risk factors of severe COVID-19, it should be noted that both of these capillary beds are dysfunctional in diabetes (Lindenmeyer et al., 2007; Singh et al., 2008).

It seems likely that SARS-CoV-2 infection of pericytes is rare in individuals with a healthy microvasculature, but the situation is different if the endothelial barrier is pathologically disrupted. Breakdown of endothelial junctions and transcytosis has been described in numerous inflammatory conditions (Bonetti et al., 2003), and increased vascular leakage and resulting edema are hallmarks of inflammation. Low-level tissue inflammation, endothelial dysfunction and increased

vascular permeability and leakage have been reported in hypertension, diabetes, obesity and aging, and locally in ischemic heart and brain disease, cancer and neurodegenerative diseases (Cai and Harrison, 2000; Iantorno et al., 2014; Kwaifa et al., 2020; Nation et al., 2019; Sun et al., 2019; Sweeney et al., 2018; Viazzi et al., 2006; Virdis, 2016; Weis, 2008). All these conditions are risk factors and co-morbidities of severe COVID-19 disease. An important aspect of the COVID-19-pericyte hypothesis is therefore that these diseases and conditions increase the risk of viral passage through the endothelial barrier by promoting endothelial dysfunction and increased microvascular permeability, resulting in subsequent infection of pericytes.

An important still open question is whether SARS-CoV-2 in severely ill COVID-19 patients has actually infected pericytes. The fact that expression of ACE2 together with either TMPRSS2 or CTSB/L is sufficient to elicit S protein processing and viral entry into cultured cells (Hoffmann et al., 2020) combined with that pericytes express both ACE2 and CTSB/L suggests that pericytes could be infected. However, whether they indeed can be productively infected *in vivo* remains to be demonstrated experimentally or by examination of tissue samples from patients. We are currently investigating the presence of SARS-Cov-2 RNA in pericytes in biopsies and their organ cultures obtained from COVID-19 patients undergoing intensive care. Virus particles were recently observed near microvascular structures in postmortem samples from COVID-19 patients that had severe cardiovascular complications (Varga et al., 2020). Another recent study showed that SARS-CoV-2 can infect and multiply in human microvascular organoids that consisted of endothelial cells and PDGFRβ–positive putative pericytes (Monteil et al., 2020). It will be interesting to learn which vascular cell type(s) contained the virus in these organoids.

Pathological consequences of pericyte infection by SARS-CoV-2

While we still need to experimentally validate that pericytes can become infected by SARS-CoV-2 *in vitro* and *in vivo*, we report several observations suggesting that they may orchestrate thrombogenic responses in the microvasculature. First, we and others have shown in mouse models with pericyte hypoplasia that pericyte function is critical for vascular stability, endothelial barrier and pro-inflammatory functions

(Armulik et al., 2010; Bell et al., 2010; Daneman et al., 2010; Hong et al., 2015; Lindahl et al., 1997; Török et al., 2019). Here, we report that endothelial cells in pericyte-deficient mouse microvasculature increase VWF production and release, which should promote platelet aggregation and blood coagulation. SARS-CoV-2 in pericytes may hence cause upregulation of VWF production and release in the neighboring capillary endothelial cells. In an analogous fashion, viral infection of pericytes may thus contribute to the thrombogenicity and hypercoagulation observed in COVID-19 patients. In this context it is noteworthy that increased levels of VWF protein, activity and coagulation factor VIII were reported in a recent survey of thrombosis and coagulation parameters in patients with severe COVID-19 disease (Helms et al., 2020).

In a recent analysis of the endothelial reaction to pericyte loss, we also found upregulation of several other pro-inflammatory mediators, including angiopoietin-2 (Mäe et al, submitted). However, such pro-inflammatory endothelial changes appear to occur in the absence of severe vascular inflammation in the pericyte-deficient mice. When pericytes become infected by SARS-CoV-2, they should become targets of immune attack (Perlman and Dandekar, 2005), turning a pro-inflammatory endothelial response into fulminant microvascular inflammation. Propagation of microvascular inflammation could eventually engage a large part of the body, leading to a surge in inflammatory mediators, a cytokine storm (Jose and Manuel, 2020), as observed in many severely ill COVID-19 patients, including those in the Stockholm region intensive care cohort reported here (Table 1). Because the COVID-19-pericyte hypothesis infers that an inflammatory condition, irrespective of cause, would allow SARS-Cov-2 extravasation, it has also occurred to us that normally innocuous inflammatory reactions associated with mild irritations of the skin or mild local trauma may be enhanced in SARS-CoV-2 carriers (Galvan Casas et al., 2020).

Outlook

We posit the COVID-19-pericyte hypothesis on the basis of a combination of clinical data, single-cell transcriptomics and observations in pericyte-deficient mice. The hypothesis is testable, and it will hopefully inform and stimulate additional work aiming at filling the gaps in our data that eventually proves or disproves our

hypothesis. While several data support the hypothesis, we still lack data on pericyte infection, a void whose filling would benefit from engagement of the broad research community. A deeper analysis of the range of thrombogenicity and hypercoagulation states in severely ill COVID-19 patients is also warranted. A detailed morphological analysis of the microvascular morphology with special emphasis on inflammatory hallmarks in all organs of deceased COVID-19 patients and their correlation with ACE2 expression by pericytes would likewise be tremendously valuable.

Finally, the COVID-19-pericyte hypothesis calls for expanded discussions on potentially novel targets for therapeutic anticoagulants, including the need for drug combinations. Moreover, the hypothesis calls for introduction of much sought-after preventive therapy among at-risk patients (considering both premorbid risk factors and risk environments). Because of the proposed microvascular origin of thrombosis, inhibitors of platelet aggregation might be particularly useful (Cattaneo et al., 2020). The COVID-19-pericyte hypothesis has bearing also on the considerations of type of anti-viral therapy and its modality. As the development of vaccines is sometimes a protracted and uncertain process, systemic delivery of virus-trapping molecules, such as a soluble ACE2 protein (Monteil et al., 2020), stand out as particularly attractive in a scenario where virus spread through the blood is a key culprit for severe COVID-19 disease.

Materials and Methods

Single cell RNAseq data analysis

Mouse heart single cell data integration

ScRNAseq data were obtained from internal mouse heart single cell projects and the published Tabula Muris heart dataset (Tabula Muris et al., 2018), collectively including diverse cell types in the heart. All samples were obtained from 6-20 weeks old C57Bl6 mice. FACS-based cell capture into 384-well plates with subsequent scRNAseq data generation was conducted using the SMART-Seq2 protocol (Picelli et al., 2014) and by microfluidic-droplet-based capture by the 10X Genomics protocol. Data processing and clustering were performed using the Seurat package (v. 3.1.1). Cells containing less than 200 expressed genes were filtered out. For the SMART-

Seq2 data, cells that generated less than 50,000 reads were filtered out; for the droplet platform, cells containing less than 1000 UMIs were filtered out. Furthermore, genes that were expressed by less than three cells in a dataset were removed. After removing low quality cells from the dataset, the data were normalized using the LogNormalize function, by which feature counts for each cell are divided by the total counts for that cell and multiplied by a scale factor (1 million) and then logarithmically transformed. For integration of different datasets, the integration workflow "Reciprocal PCA" in the Seurat package was implemented, which integrated overall datasets using the mutual nearest neighbor (MNN) cell pairs that shared a common set of molecular features in their PCA spaces. After integration, we obtained a total of 18,378 genes and 10,101 cells for downstream analysis. The function "FindClusters" in the Seurat package was used to identify the clusters with a resolution parameter of 0.5.

Mouse lung single cell data integration

The mouse lung datasets were obtained from internal lung single cell projects and the published Tabula Muris lung resource (Tabula Muris et al., 2018). All samples were from 10-19 weeks old C57Bl6 mice. Data integration and clustering analysis for the lung were performed with the same methods as for the mouse heart data described above. We obtained a total of 20,114 genes and 11,085 cells in the integrated lung dataset.

Mouse brain single cell data integration

Mouse brain datasets were integrated from two internal brain single-cell projects and one published (the Tabula Muris brain resource) (Tabula Muris et al., 2018). The internal datasets included one unpublished and one previously published brain vasculature dataset (He et al., 2018). The cells were from 10-19 weeks old C57Bl6 mice. Data integration and clustering analysis were performed with the same methods as for the mouse heart and lung data described above. We obtained a total of 12,940 cells and 17,779 genes in the integrated brain dataset.

Bar plot visualization of integrated datasets

In order to provide detailed visualizations of the primary gene expression data cell-by-cell for each cluster of the integrated dataset, we created bar plots using the normalized counts from each cell. In these graphs, a bar represents a cell and is colored according to its data source. The data source abbreviations "ss2" and "droplet" in the legend represent the SMART-Seq2 protocol and microfluidic-droplet-based capture by the 10X Genomics protocol, respectively. For the integrated dataset of lung, "TJA_ss2", "CBZ_ss2" and "H_droplet" represent in-house unpublished datasets; "TM_ss2" and "TM_droplet" represent published Tabula Muris data (Tabula Muris et al., 2018). For the integrated dataset of heart, "L_ss2", "S_ss2" and "H_droplet" represent in-house unpublished datasets; "TM_ss2" and "TM_droplet" represent published Tabula Muris data. For the integrated dataset of brain, "C_ss2" and "K_droplet" represent in-house unpublished datasets; "TM_ss2" represents published Tabula Muris data.

Human heart

The human heart single cell data were extracted from a published study (Wang et al., 2020a), and only cells from healthy donors were included in the current analysis. The Seurat package (version 3.1.1) was used for raw data processing, filtering, normalization, clustering and further downstream analysis (Butler et al., 2018). Cells that had less than 500 expressed genes were filtered out. Genes expressed in less than 10 cells were also filtered out. In total, 8383 single cells from 14 previously healthy organ donors (12 males and 2 males) qualified for downstream analysis. The gene expression levels in each cell were normalized to a total read counts of 100,000 per cell. The top 2,000 variable genes in the dataset were used for linear dimensional reduction of the data using the PCA method. The first 30 principal components were used for UMAP visualization and clustering of the cells using default parameters in Seurat pipeline.

Human lung

The human lung single cell data were obtained from a published study (Reyfman et al., 2019). In total, there were 76,070 qualified single cells from 16 individuals (8 donors and 8 lung fibrosis patients). The Seurat package (v3.1.1) was used for data

processing. The cell type annotations shown are the same as in the original paper (Reyfman et al., 2019). To generate the UMAP layout of the data, the reciprocal PCA method in the Seurat integration pipeline was used.

Identification of pericyte contamination of other cell types

To identify pericyte contamination in other cell types, including endothelial cells, fibroblast-like cells and cardiomyocytes, we examined the expression of several previously well-characterized pericyte-specific markers, including *Kcnj8*, *Pdgfrb* and *Abcc9*. Their expression profiles in *Ace2*-positive and *Ace2*-negative cells were compared in a random selection of equal numbers of cells, and the heat map results were visualized with pheatmap package (version 1.0.12) in R software.

Mice

The following mouse strains were used: *Pdgfb*^{ret} (*Pdgfb*-tm(ret)) (Lindblom et al., 2003), *Cspg4*-DsRed (The Jackson Laboratory, Tg(Cspg4-DsRed.T1)1Akik/J, *Pdgfrb*-GFP (Gensat.org. Tg(Pdgfrb-eGFP) JN169Gsat/Mmucd) (He et al., 2016), *Cldn5*-GFP (Tg(Cldn5-GFP)Cbet/U), *Acta2*^{GFP} (The Jackson Laboratory, Tg(*Acta2*-GFP)1Pfk), *Prox1-GFP* (Tg(Prox1-EGFP)KY221Gsat/Mmcd). All mice were backcrossed on a C57BL6/J genetic background. Adult mice, about 3 months of age and of both sexes, were used for experiments. Animal protocols were approved by either the Uppsala Ethical Committee on Animal Research (permit numbers C224/12, C115/15, C111515/16), or by the Stockholm/Linköping Ethical Committee on Animal Research (permit ID 729). All animal experiments were carried out in accordance with their guidelines.

Immunofluorescence staining

Pdgfb$^{ret/+}$ and *Pdgfb*$^{ret/ret}$ *brains*

Mice under full anesthesia were euthanized by transcardial perfusion with Hanks balanced salt solution (HBSS, cat. #14025092, GIBCO) followed by 4% buffered formaldehyde (cat. #02178, Histolab). Brains were removed and post-fixed in 4% buffered formaldehyde for 4 h at 4 °C. Sagittal and coronal vibratome sections (50-75 µm) were incubated in blocking/permeabilization solution (1% bovine serum

albumin, 2.5% donkey serum, 0.5% Triton X-100 in PBS) overnight at 4 °C, followed by incubation in primary antibody solution for two nights at 4 °C, and subsequently in secondary antibody (Jackson ImmunoResearch and Invitrogen) solution, overnight at 4 °C. A list of the used primary antibodies is presented in Supplementary Table 1. Sections were mounted in ProLong Gold Antifade mounting medium (cat. #P36930, Life Technologies). Micrographs were taken with a Leica TCS SP8 confocal microscope (Leica Microsystems). All confocal images are represented as maximum intensity projections and were adjusted for brightness and contrast using Fiji v1.52p and Adobe Photoshop CC 2019.

Blood-brain barrier permeability

For blood-brain barrier integrity assessment, dextran (100 µg/g body weight) conjugated to tetramethylrhodamine (cat. #D1818, Life Technologies) was injected intravenously into the tail vein 16 hours before sacrifice, respectively (Armulik et al., 2010). For tracer *in situ* analysis, anaesthetized animals were perfused transcardially for 5 min with HBSS followed by 4 min with 4% buffered formaldehyde. Where after the brains were processed as described under *Immunofluorescence staining.*

Cryo-sections from brain, heart and lung

Tissues were harvested from euthanized mice without perfusion and fixed by immersion in 4% formaldehyde for 4-12h at 4 °C, followed by immersion in 20% sucrose/PBS solution for at least 24h at 4°C. Thereafter, tissues were embedded for cryo-sectioning and sectioned on a CryoStat NX70 (ThermoFisher Scientific) to 14 or 30 µm thick sections collected on SuperFrost Plus glass slides (Metzler Gläser). Sections were allowed to thaw at RT and thereafter blocked for > 60 min at RT with blocking-buffer (serum-free protein blocking solution, DAKO), supplemented with 0.2% Triton X-100 (Sigma Aldrich), followed by sequentially incubation with primary antibodies (overnight at 4 °C) (Suppl Table 1) and corresponding fluorescently conjugated secondary antibodies (1h at RT) together with 10 µg/ml *Hoechst 33342* (trihydrochloride, trihydrate, ThermoFisher Scientific). Sections were mounted with

ProLong Gold Antifade mounting medium, and micrographs acquired and graphically handled as described above.

Legends to Figures, Tables and Videos

Figure 1: ACE2 expression in pericytes and venous SMC in the adult brain.

A-B. Excerpts from http://betsholtzlab.org/VascularSingleCells/database.html showing the expression of *Ace2* in individual cells (left) and average expression in cell types (right). **B.** Magnified view of indicated part of **A** comparing the expression of *Ace2*, *Cnn1* and *Kncj8*. **C.** Expression of selected known pericyte specific markers in 23 *Ace2*-positive endothelial cells (top) and 23 randomly selected *Ace2*-negative endothelial cells (bottom). Colors indicate pericyte marker as shown and the frequency of their expression is shown in the tables. **D.** IF detection of ACE2 and CD31 in cortex from *Pdgfrb*-GFP reporter mouse brain. Arrows point at *Pdgfrb*-GFP/ACE2 double-positive pericytes. Scale bars: 25 μm. **E.** The expression of known pericyte markers in *ACE2*+ cells from developing human prefrontal cortex. **F**. Heat map display of gene expression in two *ACE2*+ cells and five endothelial cells retrieved from a human glioblastoma scRNAseq dataset.

Figure 2: ACE2 expression in pericytes in the adult mouse heart.

A. UMAP visualization of the integrated scRNASeq data from mouse heart. Coloring is based on cluster assignment and cellular annotations are based on canonical marker expression. **B**. UMAP display of *Ace2* gene expression (dark color represents higher expression). Heart cells were annotated and colored based on their respective cell types (left). **C**. Bar plots of *Ace2* and *Pdgfrb* expression in the same cluster numbers as depicted in the UMAP visualization. Each bar represents a single cell and is colored according to the indicated data source (see Materials and Methods). Information below the x-axis shows cluster numbers and amount of cells from each data source. The y-axis shows the normalized expression values. **D.** IF staining of heart tissue from *Pdgfrb*-GFP reporter mice using antibodies against ACE2 and CD31. Arrows in top panels indicate GFP/ACE2 double positive pericytes. Asterisks indicate

ACE2-negative pericytes. In the lower panels, three individual pericytes with different ACE2 intensity are numbered. Arrowheads point at GFP/ACE2 double-positive pericyte processes. V denotes a vein. Scale bars: 25 μm.

Figure 3: ACE2 expression in pericytes in the adult human heart.

A. UMAP visualization of human heart cells. Colors indicate cluster assignment. Annotations were based on the expression of canonical markers for each indicated cell type. The pericyte cluster (#8) is denoted by a red arrow. The endothelial cluster (#3) is denoted by a black arrow. **B**. Bar plots of the normalized expression levels of *ACE2* and the indicated cell type markers in the same clusters as displayed in the UMAP plot. Each bar represents a cell. Arrows indicate the pericyte cluster. **C**. The expression of known pericyte markers in 77 *ACE2* -positive endothelial cells (top) and 77 *ACE2*-negative endothelial cells (bottom). Each bar is a cell and marker expression is piled up. For each group, statistics of pericyte (PC) markers is summarized in the corresponding table, including numbers and percentages of cells with no pericyte marker expressed, one or more pericyte marker, or two or more pericyte markers (indicated by # and *), respectively.

Figure 4: ACE2 expression in adult mouse lung.

A. UMAP visualization of the integrated scRNASeq data from mouse lung (left) with *Ace2* expression overlay (right, darker color represents higher expression). Colors indicate cluster assignment. Annotations were based on the expression of canonical markers for each indicated cell type. For all panels, black arrows point at AT-2 and multiciliated airway epithelial clusters, and red arrows point at the pericyte cluster. **B**. Bar plots showing expression of the indicated genes across clusters. Each bar represents a single cell and is colored according to the indicated data source (see Materials and Methods). Arrows highlight the clusters corresponding to AT-2 cells (left row of arrow) and multiciliated airway epithelial cells (right row of arrows). **C**. IF staining of ACE2 and CD31 in mouse lung tissue form a *Acta2*-GFP:*Cspg4*-dsRED double reporter mouse. Arrows point at ACE2-positive cells in the alveolar region consistent with the location of AT-2 cells. Br: bronchi, V: vein. Lower panels are insets from upper panel as indicated. Scale bar: 50 μm.

Figure 5. Von Willebrand Factor (VWF) IF staining in brains of *Pdgfb*$^{ret/ret}$ mice.

A. Bar plot illustrating *Vwf* expression in endothelial cells from *Pdgfb*$^{+/+}$, *Pdgfb*$^{ret/+}$ and *Pdgfb*$^{ret/ret}$ brains. **B-C.** IF staining of mouse cortex vasculature in *Pdgfb*$^{ret/+}$ and *Pdgfb*$^{ret/ret}$ mice with antibodies against (**B**) VWF, PDGFRB and ACTA2, and (**C**) PODXL, PDGFRB and VWF). a, arterioles. v, venules. Note that in controls, capillaries covered by PDGFRB-positive pericytes are VWF-negative, whereas the dilated pericyte-deficient capillaries in *Pdgfb*$^{ret/ret}$ brain are strongly VWF-positive. **C**. Normal brain capillaries (PODXL labels endothelial cells) covered by PDGFRB-positive pericytes are essentially VWF-negative (arrow points at location of a few Weibel-Palade bodies). In contrast, the pericyte-deficient capillaries in *Pdgfb*$^{ret/ret}$ brain show dense content of Weibel-Palade bodies and local "halo" (arrows) of VWF released into the tissue interstitium. Scale bar: 50 μm.

Figure 6. Platelet adhesion and aggregation in *Pdgfb*$^{ret/ret}$ vessels.

A. Visualization of platelets using anti-CD41 and fibrinogen (FBG) leakage and fibrin deposition in blood vessels (CD31; PECAM1) of *Pdgfb*$^{ret/ret}$ mouse brains. Arrows in the top panel point at a fibrin clot. Arrows in the bottom panel highlight platelets and local fibrin deposition. **B.** VWF release into the interstitium coincides with 70 kDa dextran tracer leakage (red) into the brain parenchyma (yellow arrows) and COL4 (COL4A1) visualizes the basement membrane of the vasculature. CD13 (ANPEP) visualizes residual mural cells. Note the anti-correlation between presence of mural cells and VWF expression. Scale bar is 25 μm in **A** and 50 μm in **B.**

Figure 7. The COVID-19-pericyte hypothesis. The schematic illustration of the COVID-19-pericyte hypothesis depicts a healthy vasculature with low risk of pericyte infection (1), a vasculature in an individual in a COVID-19 risk group with a disrupted endothelial barrier (2); and a SARS-CoV-2 infection of pericytes leading to enhanced expression of Von Willebrand Factor (VWF), platelet aggregation, fibrin deposition and eventually vascular inflammation (3). In the normal, healthy vasculature (1), the intact endothelial barrier precludes SARS-CoV-2 virus to get in contact with the Ace2-expressing pericytes localized behind the endothelial barrier. In individuals with a

leaky barrier (2), SARS-CoV-2 can infect pericytes, which in turn causes neighboring endothelial cells to upregulate VWF production, eventually leading to the vascular symptoms observed in many severely ill COVID-19 patients (3).

Table 1: Clinical, inflammatory and coagulation parameters in 20 ICU-admitted Covid-19 patients.

Continuous parameters depicted as median (range), categorical parameters as number (%). Intensive Care Unit (ICU), ratio arterial oxygen tension (kPa)/ fraction inspired oxygen (FiO_2) (PFI), C-reactive protein (CRP), procalcitonin (PCT), interleukin-6 (IL-6), interleukin-1 (IL-1), tumour necrosis factor alpha (TNF-alpha), internationalized normalized ratio (INR), activated partial thromboplastin time (APTT). Risk factors include renal disease, hypertension, cardiovascular disease, diabetes mellitus, chronic pulmonary disease and immunosuppressive therapy (Fang et al., 2020; Guan et al., 2020; Yang et al., 2020).

Supplementary Figure 1. *Ace2* mRNA in brain cells other than mural cells is due to pericyte-contamination

A. Excerpts from http://betsholtzlab.org/VascularSingleCells/database.html showing bar plots across the VSMC subtypes from a list of arterial VSMC-specific genes that anti-correlate with *Ace2*. Red arrows point at the *Ace2*-negative part of the cluster. **B**. Heat map display of pericyte and fibroblast markers in *Ace2*-positive (*Ace2+*) and *Ace2*-negative (*Ace2-*) FB2 fibroblasts and enriched genes in the *Ace2*+ cells. **C**. Heat map display of markers of different vascular and perivascular cells in *Ace2*+ and *Ace2*- endothelial cells. Only pericyte markers are enriched in *Ace2*+ endothelial cells, not arterial VSMCs or astrocyte markers. **D.** Meat map display of the 50 top enriched genes in the three *Ace2*+ cells (black arrowheads) without pericyte marker expression does not reveal a statistically significant commonality between these cells. Most of the genes listed in **D** are highly expressed in neurons, suggesting an RNA smearing artifact. **E.** UMAP visualization of the integrated scRNASeq data from mouse brain (left) with (**F**) *Ace2* expression overlay (right, darker color represents higher expression). **G**. Bar plots of the normalized expression levels of *Ace2* in each cluster. Each bar represents a single cell and is colored according to the indicated

data source (see Materials and Methods). Arrows of different colors in **E** and **G** highlight the corresponding *Ace2*+ clusters in the UMAP and bar plot displays.

Supplementary Figure 2. Immunofluorescence localization of ACE2 protein expression in the adult mouse brain cortex.

Confocal microscopy images of sections from brain cortex in *Pdgfrb*-GFP mouse brains stained with the indicated antibodies and nuclear marker. The images show ACE2 protein expression specifically in microvascular mural cells, including pericytes and VSMCs of venules and arterioles. The red frame indicates images shown in Fig 1D.

Supplementary Figure 3. *Ace2* expression in mouse heart endothelial cells is due to pericyte contamination.

A. Heat map overview of the expression of pericyte and endothelial markers in *Ace2*+ pericytes and *Ace2*+ and *Ace2*- endothelial cells in the adult mouse heart. Arrows indicate the position of three *Ace2*+ cells without other known pericyte markers. **B**. The expression of known pericyte-specific markers in the 21 *Ace2*-positive endothelial cells (top) and 21 randomly selected *Ace2*-negative endothelial cells (bottom). The expression of markers in the same cell is piled up. **C.** Heat map overview of the top enriched genes in the three *Ace2*-positive cells (arrow highlighted) without other known pericyte marker expression. There was no apparent common gene profile among the three cells, suggesting that they do not represent a specific cell type or cell state.

Supplementary Figure 4. Immunofluorescence localization of ACE2 protein expression in the adult mouse heart.

Confocal microscopy images of sections from heart in *Pdgfrb*-GFP mice stained with the indicated antibodies and nuclear markers. The images show ACE2 protein expression specifically in capillary pericytes and not present in VSMCs of larger vessels with the possible exception of veins close to the cardiac valves. This analysis also indicates that ACE2 expression levels vary between individual pericytes, and that this may be proportionally different in different regions of the heart (a higher

proportion of ACE2 positive pericytes was observed in capillaries in the proximity of the cardiac valves). The red frame indicates images shown at the bottom of the figure. Arrows point at GFP/ACE2 double positive cells. Scale bar: 100 μm.

Supplementary Figure 5. Immunofluorescence localization of ACE2 protein expression in the adult mouse lung.

Confocal microscopy images of sections from lung in *Acta2*-GFP:*Cspg4*-dsRed double reporter mice stained with the indicated antibodies and nuclear markers. The images show ACE2 protein expression specifically in the bronchial epithelium and in scattered cells with alveolar localization consistent with the position of AT-2 cells. Arrows point at strongly ACE2-positive bronchial (Br) epithelium. Scale bar: 100 μm.

Supplementary Figure 6. ***ACE2* expression in the human lung.**

A. UMAP visualization of human lung scRNAseq data (left) with cluster annotations taken from the original paper and its marker basis in the text box (top 10 markers for each cell type) (Reyfman et al., 2019). *ACE2* expression superimposed onto the UMAP image (right). **B.** Bar plot display of *ACE2* mRNA shows that it is localized to the clusters annotated as AT-2 (*SFTPC*+), basal (*KRT5*+), multiciliated (*FOXJ1*+) and club (*SCGB1A*+) cells.

Supplementary Figure 7. Co-expression analysis of *Ace2, Tmrpss2, Ctsl and Ctsb* in mouse lung, brain and heart.

Bar plots overview of *Ace2, Tmrpss2, Ctsl and Ctsb* expression across the scRNAseq meta-analysis datasets of lung, brain and heart. Each bar represents a single cell and is colored according to the indicated data source (see Materials and Methods). Cluster annotations have been described in previous figures. Arrows point at the Ace2+ clusters, which in lung represent AT-2 (left) and multiciliated cells (right), in brain: from left to right, pericytes, arteriolar VSMCs, venous VSMCs and pericyte-contaminated endothelial cells, and in heart: pericytes.

Supplementary Figure 8. VWF immunofluorescence analysis shows specific localization to Weibel–Palade bodies. Localization of VWF staining to rod-shaped

vesicles (Weibel-Palade bodies) in the endothelial cytoplasm, i.e. underneath the CD31-positive endothelial membrane, which in turn is underneath the ACTA2-positive VSMC coat of a brain arteriole in a control (*Pdgfb*$^{ret/+}$) mouse. This staining served as a control for the specificity of the antibody and quality of the immunofluorescence analysis. See also Supplementary Video 1. Scale bar: 50 μm.

Supplementary Table 1.

List of used antibodies.

Supplementary Video 1. VWF immunofluorescence analysis shows specific localization to Weibel–Palade bodies. Z-scan of the arteriole shown in Supplementary Figure 8 provides a clear view of the localization of the VWF-positive vesicles in the endothelial cytoplasm. Video download is available at http://betsholtzlab.org/Publications/2020/SupplVideo1.html

Acknowledgements

We thank Cecilia Olsson, Pia Peterson, Jana Chmielniakova, Helene Leksell, Sonja Gustafsson, Byambajav Buyandelger and Elisabeth Raschperger for technical help. This study was supported by grants from the Swedish Cancer Society (C.B., U.L.), the Swedish Research Council (C.B., U.L), the Swedish Brain Foundation (C.B., U.L.), the Erling-Persson Family Foundation (C.B., U.L.), Knut and Alice Wallenberg Foundation (C.B., T.M.), The European Union (C.B.), the Leducq Foundation (C.B.), the Louise Jeantet Prize (C.B.), The Anders Jahre Medical Prize (C.B.) and ERC advanced grant (C.B.) and consolidator grant (T.M.). C.B. and E.H. were supported by grants from AstraZeneca through the ICMC. S.S. was supported by a postdoctoral fellowship from the Deutsche Forschungsgemeinschaft (STR 1538/1-1) and a non-stipendiary long-term fellowship from the European Molecular Biology Organization (ALTF 86-2017).

Author contributions

C.B. conceived the COVID-19-pericyte hypothesis and developed it together with T.A., X-R.P., L.I.E. and U.L. L.H. did the bioinformatics analysis. M.A.M. performed

analyses of *Pdgfb* mutant mice with help from E.V.L. and K.N. Y.S. designed the scRNAseq meta-analysis pipeline and used it together with R.P. L.M. did the ACE2 immunofluorescence analysis. M.J.F and A.O. explored and analyzed ICU patient data. L.M., M.A.M., J.L., G.G., L.Z., Y.X., S.L., G.M. S.S., A.O., M.R., A.A., J.B. M.V., K.B., E.H., K.A. and T.M. provided unpublished scRNAseq data. C.B. assembled the data. C.B. and U.L. wrote the manuscript with significant input fro K.A. All authors reviewed and edited the text.

References

Grey's anatomy, 41st edn (Elsevier).

Aird, W.C. (2007). Phenotypic heterogeneity of the endothelium: I. Structure, function, and mechanisms. Circ Res *100*, 158-173.

Armulik, A., Genove, G., and Betsholtz, C. (2011). Pericytes: developmental, physiological, and pathological perspectives, problems, and promises. Dev Cell *21*, 193-215.

Armulik, A., Genove, G., Mae, M., Nisancioglu, M.H., Wallgard, E., Niaudet, C., He, L., Norlin, J., Lindblom, P., Strittmatter, K.*, et al.* (2010). Pericytes regulate the blood-brain barrier. Nature *468*, 557-561.

Batlle, D., Soler, M.J., Sparks, M.A., Hiremath, S., South, A.M., Welling, P.A., Swaminathan, S., Covid, Ace2 in Cardiovascular, L., and Kidney Working, G. (2020). Acute Kidney Injury in COVID-19: Emerging Evidence of a Distinct Pathophysiology. J Am Soc Nephrol. in press

Bell, R.D., Winkler, E.A., Sagare, A.P., Singh, I., LaRue, B., Deane, R., and Zlokovic, B.V. (2010). Pericytes control key neurovascular functions and neuronal phenotype in the adult brain and during brain aging. Neuron *68*, 409-427.

Bikdeli, B., Madhavan, M.V., Jimenez, D., Chuich, T., Dreyfus, I., Driggin, E., Nigoghossian, C., Ageno, W., Madjid, M., Guo, Y.*, et al.* (2020). COVID-19 and Thrombotic or Thromboembolic Disease: Implications for Prevention, Antithrombotic Therapy, and Follow-up. J Am Coll Cardiol. in press

Bonetti, P.O., Lerman, L.O., and Lerman, A. (2003). Endothelial dysfunction: a marker of atherosclerotic risk. Arterioscler Thromb Vasc Biol *23*, 168-175.

Braet, F., and Wisse, E. (2002). Structural and functional aspects of liver sinusoidal endothelial cell fenestrae: a review. Comp Hepatol *1*, 1.

Butler, A., Hoffman, P., Smibert, P., Papalexi, E., and Satija, R. (2018). Integrating single-cell transcriptomic data across different conditions, technologies, and species. Nat Biotechnol *36*, 411-420.

Cai, H., and Harrison, D.G. (2000). Endothelial dysfunction in cardiovascular diseases: the role of oxidant stress. Circ Res *87*, 840-844.

Cattaneo, M., Bertinato, E.M., Birocchi, S., Brizio, C., Malavolta, D., Manzoni, M., Muscarella, G., and Orlandi, M. (2020). Pulmonary Embolism or Pulmonary Thrombosis in COVID-19? Is the Recommendation to Use High-Dose Heparin for Thromboprophylaxis Justified? Thromb Haemost. in press

Chen, L., Li, X., Chen, M., Feng, Y., and Xiong, C. (2020a). The ACE2 expression in human heart indicates new potential mechanism of heart injury among patients infected with SARS-CoV-2. Cardiovasc Res *116*, 1097-1100.

Chen, W., Lan, Y., Yuan, X., Deng, X., Li, Y., Cai, X., Li, L., He, R., Tan, Y., Deng, X.*, et al.* (2020b). Detectable 2019-nCoV viral RNA in blood is a strong indicator for the further clinical severity. Emerg Microbes Infect *9*, 469-473.

Chistiakov, D.A., Orekhov, A.N., and Bobryshev, Y.V. (2015). Endothelial Barrier and Its Abnormalities in Cardiovascular Disease. Front Physiol *6*, 365.

Claesson-Welsh, L. (2015). Vascular permeability--the essentials. Ups J Med Sci *120*, 135-143.

Cohen, J. (2020). From mice to monkeys, animals studied for coronavirus answers. Science *368*, 221-222.

Daneman, R., Zhou, L., Kebede, A.A., and Barres, B.A. (2010). Pericytes are required for blood-brain barrier integrity during embryogenesis. Nature *468*, 562-566.

Diao, B., and al., e. (2020). Human kidney is a target for novel severe acute respiratory syndrome coronavirus 2 [SARS-CoV-2] infection. MedRxiv.

Fang, L., Karakiulakis, G., and Roth, M. (2020). Are patients with hypertension and diabetes mellitus at increased risk for COVID-19 infection? Lancet Respir Med *8*, e21.

Fehr, A.R., and Perlman, S. (2015). Coronaviruses: an overview of their replication and pathogenesis. Methods Mol Biol *1282*, 1-23.

Galvan Casas, C., Catala, A., Carretero Hernandez, G., Rodriguez-Jimenez, P., Fernandez Nieto, D., Rodriguez-Villa Lario, A., Navarro Fernandez, I., Ruiz-Villaverde, R., Falkenhain, D., Llamas Velasco, M.*, et al.* (2020). Classification of the cutaneous manifestations of COVID-19: a rapid prospective nationwide consensus study in Spain with 375 cases. Br J Dermatol.

Guan, W.J., Ni, Z.Y., Hu, Y., Liang, W.H., Ou, C.Q., He, J.X., Liu, L., Shan, H., Lei, C.L., Hui, D.S.C.*, et al.* (2020). Clinical Characteristics of Coronavirus Disease 2019 in China. N Engl J Med *382*, 1708-1720.

He, L., Vanlandewijck, M., Mae, M.A., Andrae, J., Ando, K., Del Gaudio, F., Nahar, K., Lebouvier, T., Lavina, B., Gouveia, L*., et al.* (2018). Single-cell RNA sequencing of mouse brain and lung vascular and vessel-associated cell types. Sci Data *5*, 180160.

He, L., Vanlandewijck, M., Raschperger, E., Andaloussi Mae, M., Jung, B., Lebouvier, T., Ando, K., Hofmann, J., Keller, A., and Betsholtz, C. (2016). Analysis of the brain mural cell transcriptome. Sci Rep *6*, 35108.

Helms, J., Tacquard, C., Severac, F., Leonard-Lorant, I., Ohana, M., Delabranche, X., Merdji, H., Clere-Jehl, R., Schenck, M., Fagot Gandet, F*., et al.* (2020). High risk of thrombosis in patients with severe SARS-CoV-2 infection: a multicenter prospective cohort study. Intensive Care Med. In press

Hoffmann, M., Kleine-Weber, H., Schroeder, S., Kruger, N., Herrler, T., Erichsen, S., Schiergens, T.S., Herrler, G., Wu, N.H., Nitsche, A*., et al.* (2020). SARS-CoV-2 Cell Entry Depends on ACE2 and TMPRSS2 and Is Blocked by a Clinically Proven Protease Inhibitor. Cell *181*, 271-280 e278.

Hong, J., Tobin, N.P., Rundqvist, H., Li, T., Lavergne, M., Garcia-Ibanez, Y., Qin, H., Paulsson, J., Zeitelhofer, M., Adzemovic, M.Z*., et al.* (2015). Role of Tumor Pericytes in the Recruitment of Myeloid-Derived Suppressor Cells. J Natl Cancer Inst *107*.

Iantorno, M., Campia, U., Di Daniele, N., Nistico, S., Forleo, G.B., Cardillo, C., and Tesauro, M. (2014). Obesity, inflammation and endothelial dysfunction. J Biol Regul Homeost Agents *28*, 169-176.

Jaffe, E.A. (1987). Cell biology of endothelial cells. Hum Pathol *18*, 234-239.

Jose, R.J., and Manuel, A. (2020). COVID-19 cytokine storm: the interplay between inflammation and coagulation. Lancet Respir Med. In press

Kim, J.M., Chung, Y.S., Jo, H.J., Lee, N.J., Kim, M.S., Woo, S.H., Park, S., Kim, J.W., Kim, H.M., and Han, M.G. (2020). Identification of Coronavirus Isolated from a Patient in Korea with COVID-19. Osong Public Health Res Perspect *11*, 3-7.

Klok, F.A., Kruip, M., van der Meer, N.J.M., Arbous, M.S., Gommers, D., Kant, K.M., Kaptein, F.H.J., van Paassen, J., Stals, M.A.M., Huisman, M.V.*, et al.* (2020). Confirmation of the high cumulative incidence of thrombotic complications in critically ill ICU patients with COVID-19: An updated analysis. Thromb Res. In press

Kwaifa, I.K., Bahari, H., Yong, Y.K., and Noor, S.M. (2020). Endothelial Dysfunction in Obesity-Induced Inflammation: Molecular Mechanisms and Clinical Implications. Biomolecules *10*.

Lazzerini, P.E., Boutjdir, M., and Capecchi, P.L. (2020). COVID-19, Arrhythmic Risk and Inflammation: Mind the Gap! Circulation. In press.

Le Berre, A., Marteau, V., Emmerich, J., and Zins, M. (2020). Concomitant acute aortic thrombosis and pulmonary embolism complicating COVID-19 pneumonia. Diagn Interv Imaging *101*, 321-322.

Leisman, D.E., Deutschman, C.S., and Legrand, M. (2020). Facing COVID-19 in the ICU: vascular dysfunction, thrombosis, and dysregulated inflammation. Intensive Care Med. In press.

Lely, A.T., Hamming, I., van Goor, H., and Navis, G.J. (2004). Renal ACE2 expression in human kidney disease. J Pathol *204*, 587-593.

Li, W., Zhang, C., Sui, J., Kuhn, J.H., Moore, M.J., Luo, S., Wong, S.K., Huang, I.C., Xu, K., Vasilieva, N.*, et al.* (2005). Receptor and viral determinants of SARS-coronavirus adaptation to human ACE2. EMBO J *24*, 1634-1643.

Liliensiek, S.J., Nealey, P., and Murphy, C. (2009). Characterization of endothelial basement membrane nanotopography in rhesus macaque as a guide for vessel tissue engineering (Mary Ann Liebert, Inc.).

Lindahl, P., Johansson, B.R., Leveen, P., and Betsholtz, C. (1997). Pericyte loss and microaneurysm formation in PDGF-B-deficient mice. Science *277*, 242-245.

Lindblom, P., Gerhardt, H., Liebner, S., Abramsson, A., Enge, M., Hellstrom, M., Backstrom, G., Fredriksson, S., Landegren, U., Nystrom, H.C*., et al.* (2003). Endothelial PDGF-B retention is required for proper investment of pericytes in the microvessel wall. Genes Dev *17*, 1835-1840.

Lindenmeyer, M.T., Kretzler, M., Boucherot, A., Berra, S., Yasuda, Y., Henger, A., Eichinger, F., Gaiser, S., Schmid, H., Rastaldi, M.P*., et al.* (2007). Interstitial vascular rarefaction and reduced VEGF-A expression in human diabetic nephropathy. J Am Soc Nephrol *18*, 1765-1776.

Lovren, F., Pan, Y., Quan, A., Teoh, H., Wang, G., Shukla, P.C., Levitt, K.S., Oudit, G.Y., Al-Omran, M., Stewart, D.J*., et al.* (2008). Angiotensin converting enzyme-2 confers endothelial protection and attenuates atherosclerosis. Am J Physiol Heart Circ Physiol *295*, H1377-1384.

Madonna, R., Balistreri, C.R., Geng, Y.J., and De Caterina, R. (2017). Diabetic microangiopathy: Pathogenetic insights and novel therapeutic approaches. Vascul Pharmacol *90*, 1-7.

Mao, L., Jin, H., Wang, M., Hu, Y., Chen, S., He, Q., Chang, J., Hong, C., Zhou, Y., Wang, D*., et al.* (2020). Neurologic Manifestations of Hospitalized Patients With Coronavirus Disease 2019 in Wuhan, China. JAMA Neurol.

Matsuyama, S., Nagata, N., Shirato, K., Kawase, M., Takeda, M., and Taguchi, F. (2010). Efficient activation of the severe acute respiratory syndrome coronavirus spike protein by the transmembrane protease TMPRSS2. J Virol *84*, 12658-12664.

Monteil, V., Kwon, H., Prado, P., Hagelkruys, A., Wimmer, R.A., Stahl, M., Leopoldi, A., Garreta, E., Hurtado Del Pozo, C., Prosper, F.*, et al.* (2020). Inhibition of SARS-CoV-2 Infections in Engineered Human Tissues Using Clinical-Grade Soluble Human ACE2. Cell. In press.

Mundi, S., Massaro, M., Scoditti, E., Carluccio, M.A., van Hinsbergh, V.W.M., Iruela-Arispe, M.L., and De Caterina, R. (2018). Endothelial permeability, LDL deposition, and cardiovascular risk factors-a review. Cardiovasc Res *114*, 35-52.

Muus, C., Luecken, M.D., Eraslan, G., Waghray, A., Heimnerg, G., and al., e. (2020). Integrated analyses of single-cell atlases reveal age, gender, and smoking status associations with cell type-specific expression of mediators of SARS-CoV-2 viral entry and highlights inflammatory programs in putative target cells. bioRxiv.

Nation, D.A., Sweeney, M.D., Montagne, A., Sagare, A.P., D'Orazio, L.M., Pachicano, M., Sepehrband, F., Nelson, A.R., Buennagel, D.P., Harrington, M.G.*, et al.* (2019). Blood-brain barrier breakdown is an early biomarker of human cognitive dysfunction. Nat Med *25*, 270-276.

Navas-Martin, S.R., and Weiss, S. (2004). Coronavirus replication and pathogenesis: Implications for the recent outbreak of severe acute respiratory syndrome (SARS), and the challenge for vaccine development. J Neurovirol *10*, 75-85.

Neuman, B.W., Adair, B.D., Yoshioka, C., Quispe, J.D., Orca, G., Kuhn, P., Milligan, R.A., Yeager, M., and Buchmeier, M.J. (2006). Supramolecular architecture of severe acute respiratory syndrome coronavirus revealed by electron cryomicroscopy. J Virol *80*, 7918-7928.

Ohishi, M., Yamamoto, K., and Rakugi, H. (2013). Angiotensin (1-7) and other angiotensin peptides. Curr Pharm Des *19*, 3060-3064.

Panigada, M., Bottino, N., Tagliabue, P., Grasselli, G., Novembrino, C., Chantarangkul, V., Pesenti, A., Peyvandi, F., and Tripodi, A. (2020). Hypercoagulability of COVID-19 patients in Intensive Care Unit. A Report of Thromboelastography Findings and other Parameters of Hemostasis. J Thromb Haemost.

Peng, L., Liu, J., Xu, W., Luo, Q., Chen, D., Lei, Z., Huang, Z., Li, X., Deng, K., Lin, B.*, et al.* (2020). SARS-CoV-2 can be detected in urine, blood, anal swabs, and oropharyngeal swabs specimens. J Med Virol.

Perlman, S., and Dandekar, A.A. (2005). Immunopathogenesis of coronavirus infections: implications for SARS. Nat Rev Immunol *5*, 917-927.

Picelli, S., Faridani, O.R., Bjorklund, A.K., Winberg, G., Sagasser, S., and Sandberg, R. (2014). Full-length RNA-seq from single cells using Smart-seq2. Nat Protoc *9*, 171-181.

Poissy, J., Goutay, J., Caplan, M., Parmentier, E., Duburcq, T., Lassalle, F., Jeanpierre, E., Rauch, A., Labreuche, J., Susen, S.*, et al.* (2020). Pulmonary Embolism in COVID-19 Patients: Awareness of an Increased Prevalence. Circulation. In press

Quartuccio, L., Semerano, L., Benucci, M., Boissier, M.C., and De Vita, S. (2020). Urgent avenues in the treatment of COVID-19: Targeting downstream inflammation to prevent catastrophic syndrome. Joint Bone Spine *87*, 191-193.

Reyfman, P.A., Walter, J.M., Joshi, N., Anekalla, K.R., McQuattie-Pimentel, A.C., Chiu, S., Fernandez, R., Akbarpour, M., Chen, C.I., Ren, Z.*, et al.* (2019). Single-Cell Transcriptomic Analysis of Human Lung Provides Insights into the Pathobiology of Pulmonary Fibrosis. Am J Respir Crit Care Med *199*, 1517-1536.

Richardson, S., Hirsch, J.S., Narasimhan, M., Crawford, J.M., McGinn, T., Davidson, K.W., and the Northwell, C.-R.C., Barnaby, D.P., Becker, L.B., Chelico, J.D*., et al.* (2020). Presenting Characteristics, Comorbidities, and Outcomes Among 5700 Patients Hospitalized With COVID-19 in the New York City Area. JAMA. In press.

Sardu, C., Gambardella, J., Morelli, M.B., Wang., X., Marfella, R., and Santulli, G. (2020). Is COVID-19 and endothelial disease? Clinical and basic evidence. Researchgate.

Sarin, H. (2010). Physiologic upper limits of pore size of different blood capillary types and another perspective on the dual pore theory of microvascular permeability. J Angiogenes Res *2*, 14.

Singh, D.K., Winocour, P., and Farrington, K. (2008). Mechanisms of disease: the hypoxic tubular hypothesis of diabetic nephropathy. Nat Clin Pract Nephrol *4*, 216-226.

Sluimer, J.C., Gasc, J.M., Hamming, I., van Goor, H., Michaud, A., van den Akker, L.H., Jutten, B., Cleutjens, J., Bijnens, A.P., Corvol, P*., et al.* (2008). Angiotensin-converting enzyme 2 (ACE2) expression and activity in human carotid atherosclerotic lesions. J Pathol *215*, 273-279.

Spiezia, L., Boscolo, A., Poletto, F., Cerruti, L., Tiberio, I., Campello, E., Navalesi, P., and Simioni, P. (2020). COVID-19-Related Severe Hypercoagulability in Patients Admitted to Intensive Care Unit for Acute Respiratory Failure. Thromb Haemost.In press.

Sun, H.J., Wu, Z.Y., Nie, X.W., and Bian, J.S. (2019). Role of Endothelial Dysfunction in Cardiovascular Diseases: The Link Between Inflammation and Hydrogen Sulfide. Front Pharmacol *10*, 1568.

Sungnak, W., Huang, N., Becavin, C., Berg, M., Queen, R., Litvinukova, M., Talavera-Lopez, C., Maatz, H., Reichart, D., Sampaziotis, F*., et al.* (2020). SARS-CoV-2 entry factors are highly expressed in nasal epithelial cells together with innate immune genes. Nat Med. In press.

Sweeney, M.D., Kisler, K., Montagne, A., Toga, A.W., and Zlokovic, B.V. (2018). The role of brain vasculature in neurodegenerative disorders. Nat Neurosci *21*, 1318-1331.

Tabula Muris, C., Overall, c., Logistical, c., Organ, c., processing, Library, p., sequencing, Computational data, a., Cell type, a., Writing, g*., et al.* (2018). Single-cell transcriptomics of 20 mouse organs creates a Tabula Muris. Nature *562*, 367-372.

Tang, N., Li, D., Wang, X., and Sun, Z. (2020). Abnormal coagulation parameters are associated with poor prognosis in patients with novel coronavirus pneumonia. J Thromb Haemost *18*, 844-847.

Török, O., Schreiner, B., Tsai, H.-C., Utz, S., Schaffenrath, J., Nassiri, S., Delorenzi, M., Aguzzi, A., Han, M.H., Greter, M*., et al.* (2019). Pericytes regulate vascular immune homeostasis in the CNS. bioRxiv.

Tucker, N.R., and al., e. (2020). Myocyte Specific Upregulation of ACE2 in Cardiovascular Disease: Implications for SARS-CoV-2 mediated myocarditis. MedRxiv.

van Sloten, T.T., Sedaghat, S., Carnethon, M.R., Launer, L.J., and Stehouwer, C.D.A. (2020). Cerebral microvascular complications of type 2 diabetes: stroke, cognitive dysfunction, and depression. Lancet Diabetes Endocrinol *8*, 325-336.

Vanlandewijck, M., He, L., Mae, M.A., Andrae, J., Ando, K., Del Gaudio, F., Nahar, K., Lebouvier, T., Lavina, B., Gouveia, L*., et al.* (2018). A molecular atlas of cell types and zonation in the brain vasculature. Nature *554*, 475-480.

Varga, Z., Flammer, A.J., Steiger, P., Haberecker, M., Andermatt, R., Zinkernagel, A.S., Mehra, M.R., Schuepbach, R.A., Ruschitzka, F., and Moch, H. (2020). Endothelial cell infection and endotheliitis in COVID-19. Lancet *395*, 1417-1418.

Viazzi, F., Leoncini, G., Ratto, E., Vaccaro, V., Tomolillo, C., Falqui, V., Parodi, A., Conti, N., Deferrari, G., and Pontremoli, R. (2006). Microalbuminuria, blood pressure load, and systemic vascular permeability in primary hypertension. Am J Hypertens *19*, 1183-1189.

Virdis, A. (2016). Endothelial Dysfunction in Obesity: Role of Inflammation. High Blood Press Cardiovasc Prev *23*, 83-85.

Wang, L., Yu, P., Zhou, B., Song, J., Li, Z., Zhang, M., Guo, G., Wang, Y., Chen, X., Han, L*., et al.* (2020a). Single-cell reconstruction of the adult human heart during heart failure and recovery reveals the cellular landscape underlying cardiac function. Nat Cell Biol *22*, 108-119.

Wang, W., Xu, Y., Gao, R., Lu, R., Han, K., Wu, G., and Tan, W. (2020b). Detection of SARS-CoV-2 in Different Types of Clinical Specimens. JAMA. In press.

Weis, S.M. (2008). Vascular permeability in cardiovascular disease and cancer. Curr Opin Hematol *15*, 243-249.

Wisse, E., Jacobs, F., Topal, B., Frederik, P., and De Geest, B. (2008). The size of endothelial fenestrae in human liver sinusoids: implications for hepatocyte-directed gene transfer. Gene Ther *15*, 1193-1199.

Yang, X., Yu, Y., Xu, J., Shu, H., Xia, J., Liu, H., Wu, Y., Zhang, L., Yu, Z., Fang, M*., et al.* (2020). Clinical course and outcomes of critically ill patients with SARS-CoV-2 pneumonia in Wuhan, China: a single-centered, retrospective, observational study. Lancet Respir Med *8*, 475-481.

Yuan, S.Y., Breslin, J.W., Perrin, R., Gaudreault, N., Guo, M., Kargozaran, H., and Wu, M.H. (2007). Microvascular permeability in diabetes and insulin resistance. Microcirculation *14*, 363-373.

Zeisel, A., Hochgerner, H., Lonnerberg, P., Johnsson, A., Memic, F., van der Zwan, J., Haring, M., Braun, E., Borm, L.E., La Manno, G.*, et al.* (2018). Molecular Architecture of the Mouse Nervous System. Cell *174*, 999-1014 e1022.

Zhong, S., Zhang, S., Fan, X., Wu, Q., Yan, L., Dong, J., Zhang, H., Li, L., Sun, L., Pan, N.*, et al.* (2018). A single-cell RNA-seq survey of the developmental landscape of the human prefrontal cortex. Nature *555*, 524-528.

Zhou, F., Yu, T., Du, R., Fan, G., Liu, Y., Liu, Z., Xiang, J., Wang, Y., Song, B., Gu, X.*, et al.* (2020). Clinical course and risk factors for mortality of adult inpatients with COVID-19 in Wuhan, China: a retrospective cohort study. Lancet *395*, 1054-1062.

Ziegler, C.G.K., Allon, S.J., Nyquist, S.K., and et.al. (2020). SARS-CoV-2 receptor ACE2 is an interferon-stimulated gene in human airway epithelial cells and is detected in specific cell subsets across tissues. Cell, CELL 11384.

Zou, X., Chen, K., Zou, J., Han, P., Hao, J., and Han, Z. (2020). Single-cell RNA-seq data analysis on the receptor ACE2 expression reveals the potential risk of different human organs vulnerable to 2019-nCoV infection. Front Med. In press

Figure 1

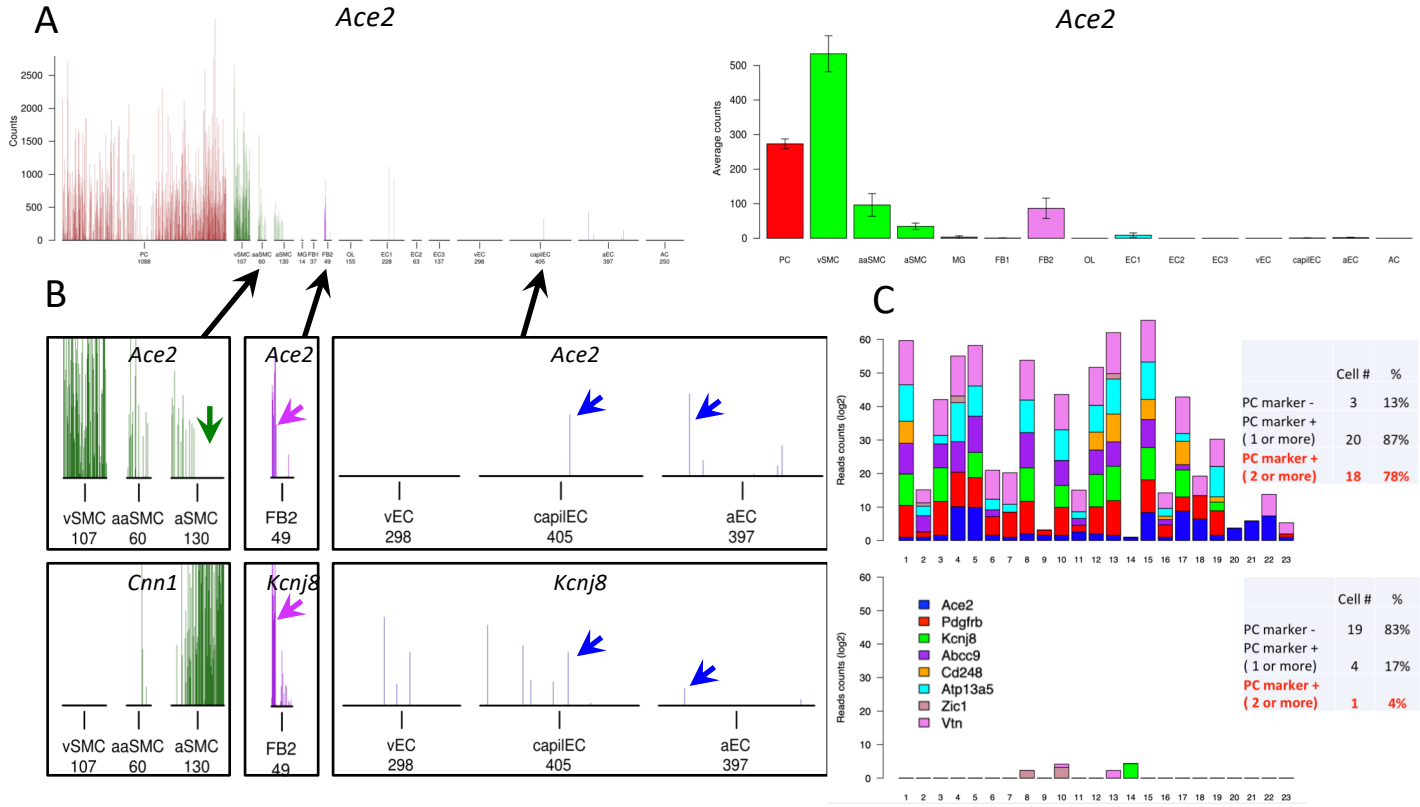

D

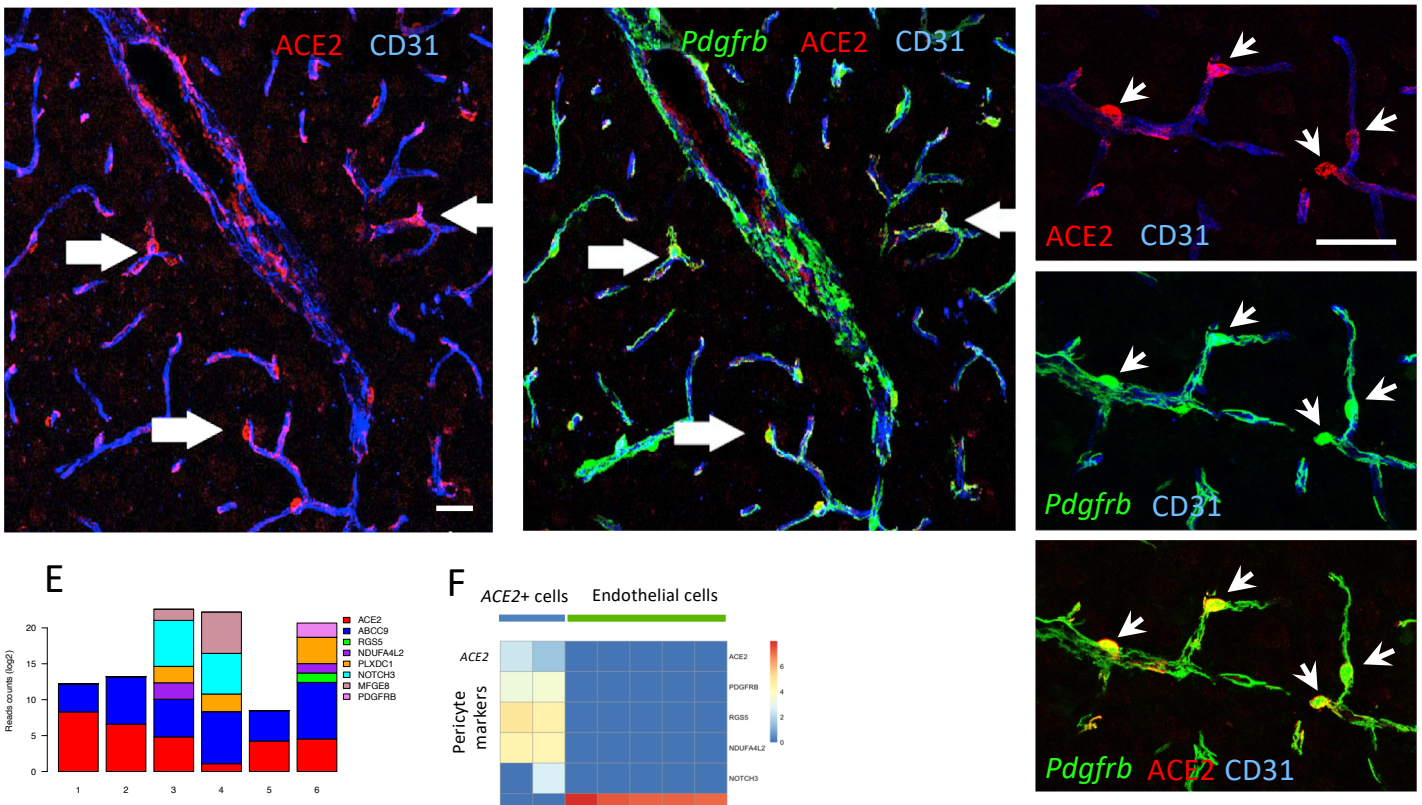

Figure 2

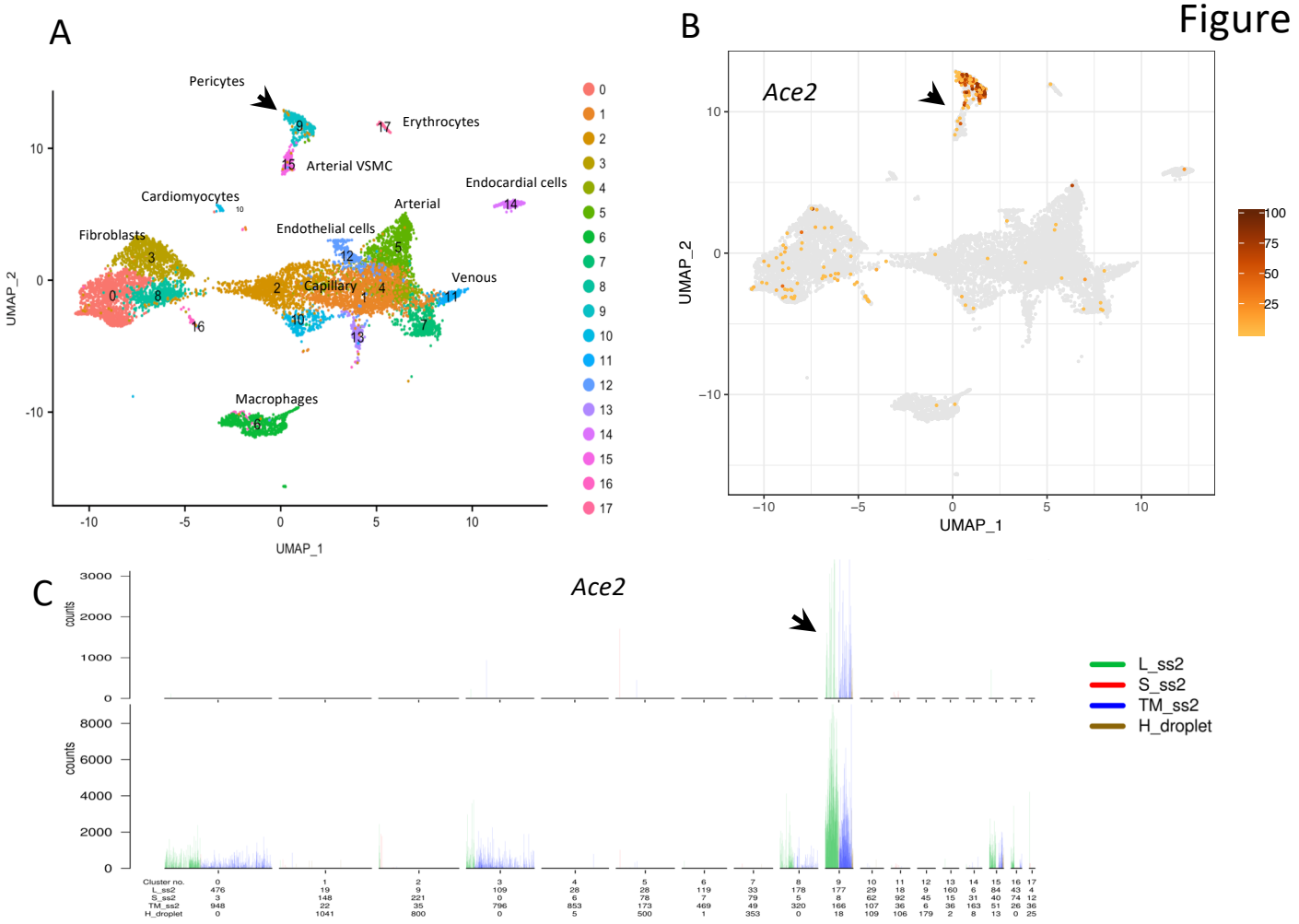

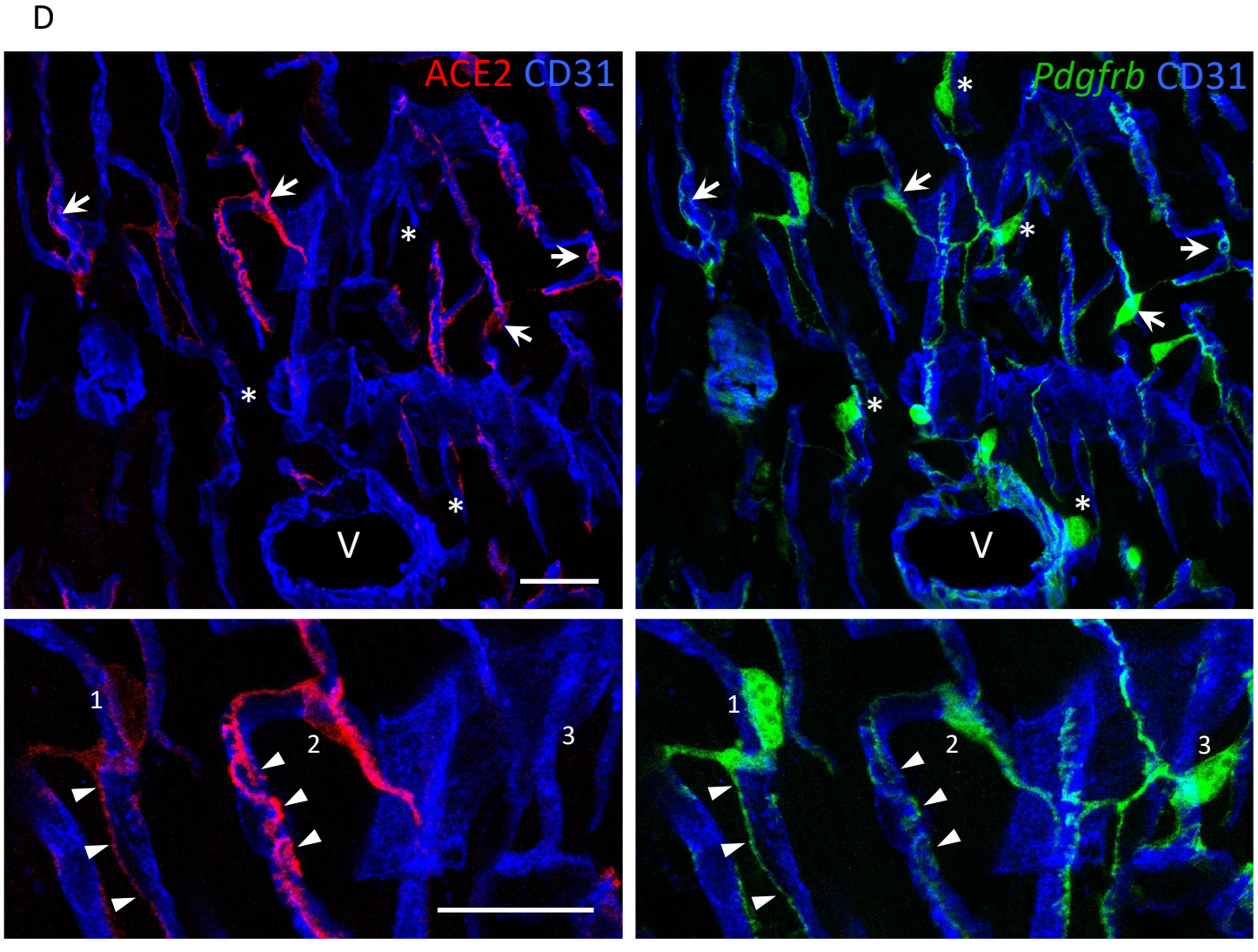

Figure 3

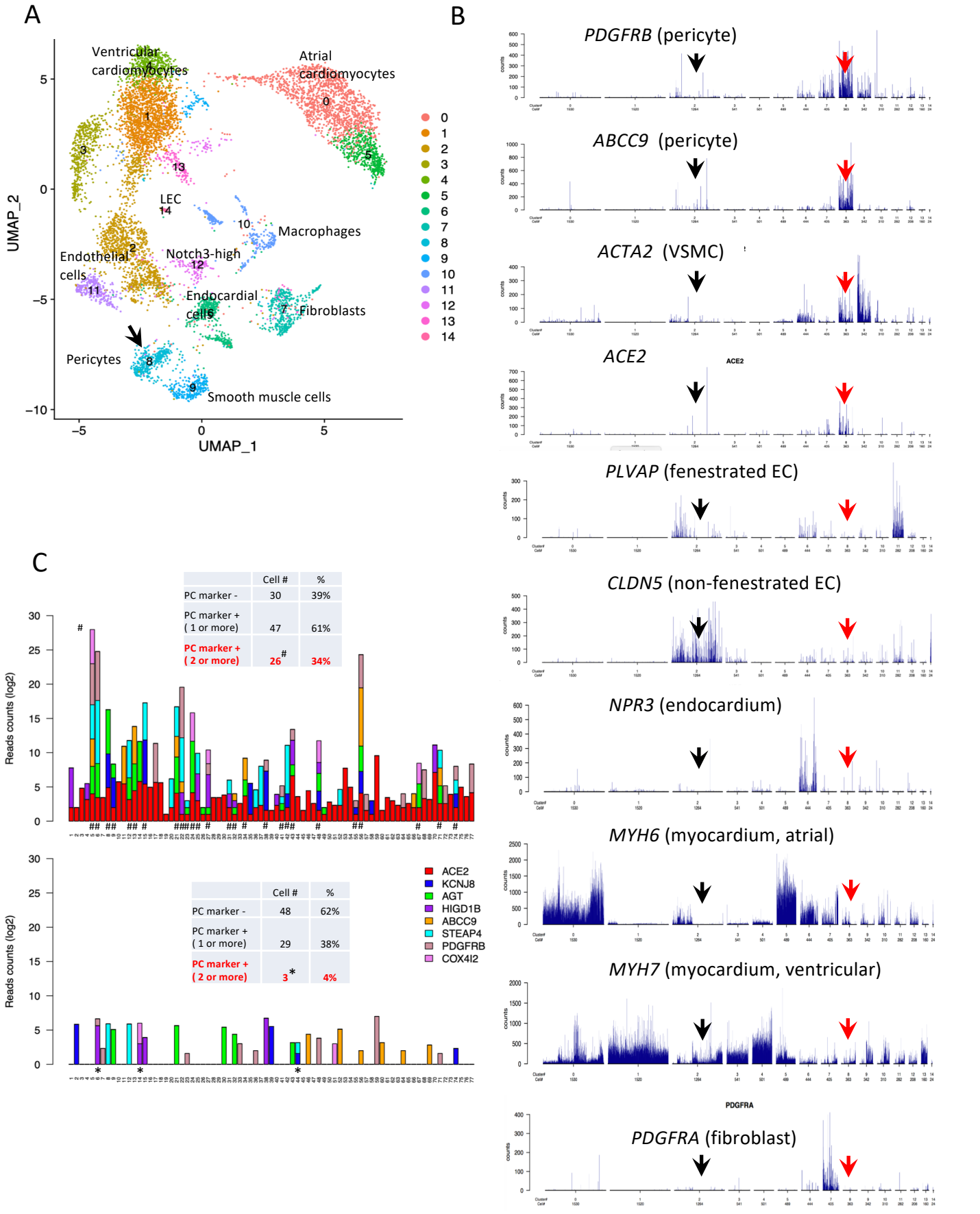

Figure 4

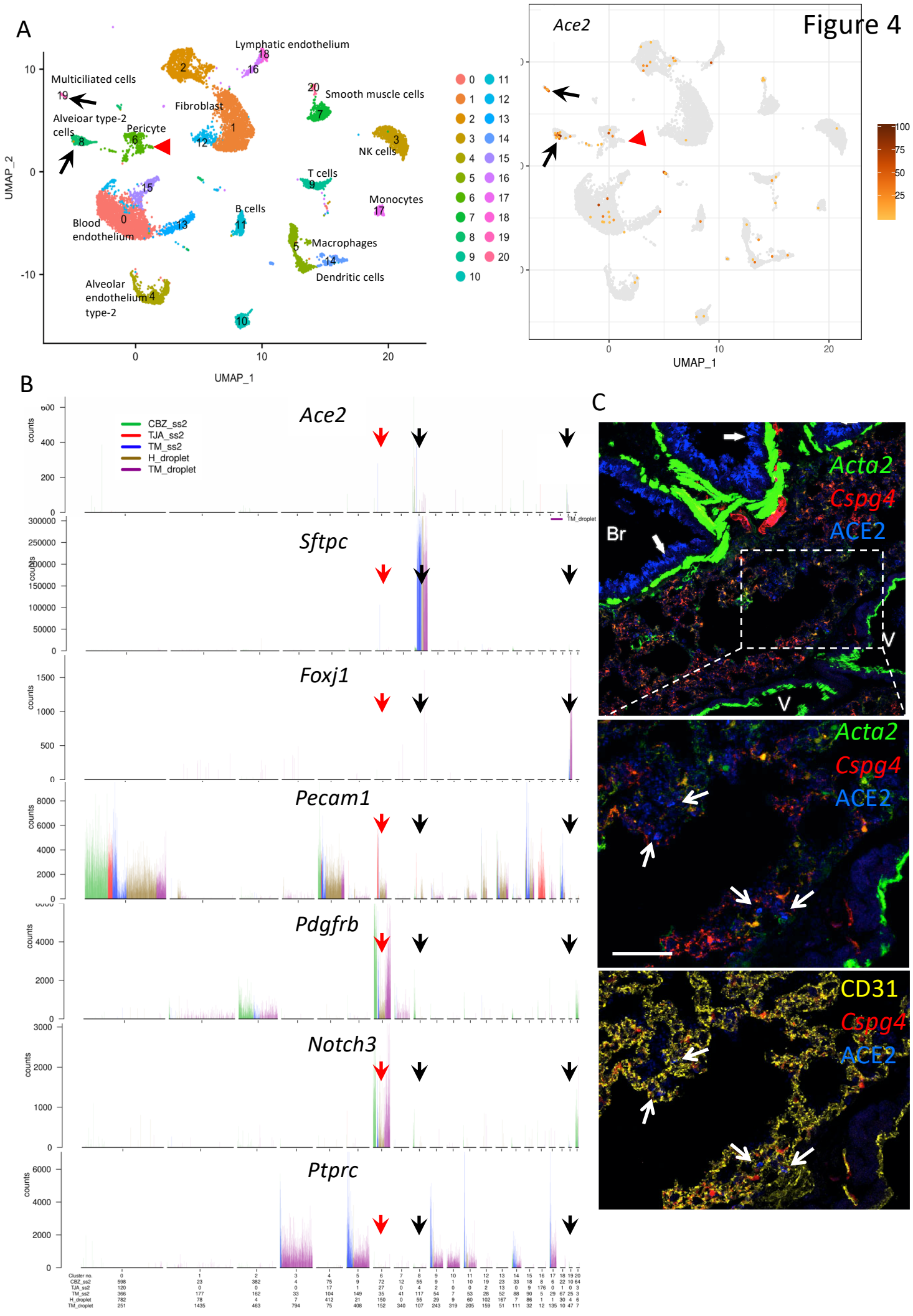
A
Lymphatic endothelium
Multiciliated cells
Fibroblast
Smooth muscle cells
Alveioar type-2 cells
Pericyte
NK cells
T cells
Monocytes
B cells
Blood endothelium
Macrophages
Dendritic cells
Alveolar endothelium type-2
UMAP_1
UMAP_2
Ace2
B
CBZ_ss2
TJA_ss2
TM_ss2
H_droplet
TM_droplet
Ace2
Sftpc
Foxj1
Pecam1
Pdgfrb
Notch3
Ptprc
counts
C
Acta2
Cspg4
ACE2
Br
V
CD31

Figure 5

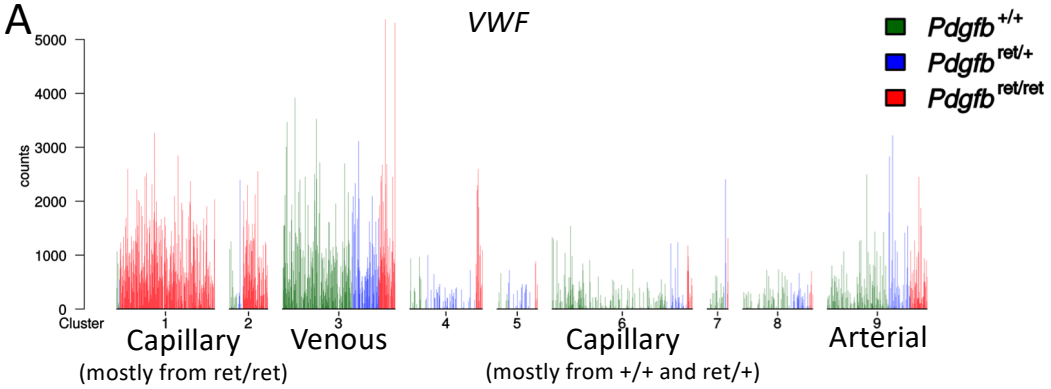
A
VWF
Pdgfb +/+
Pdgfb ret/+
Pdgfb ret/ret
counts
5000
4000
3000
2000
1000
0
Cluster
1
2
3
4
5
6
7
8
9
Capillary
(mostly from ret/ret)
Venous
Capillary
(mostly from +/+ and ret/+)
Arterial

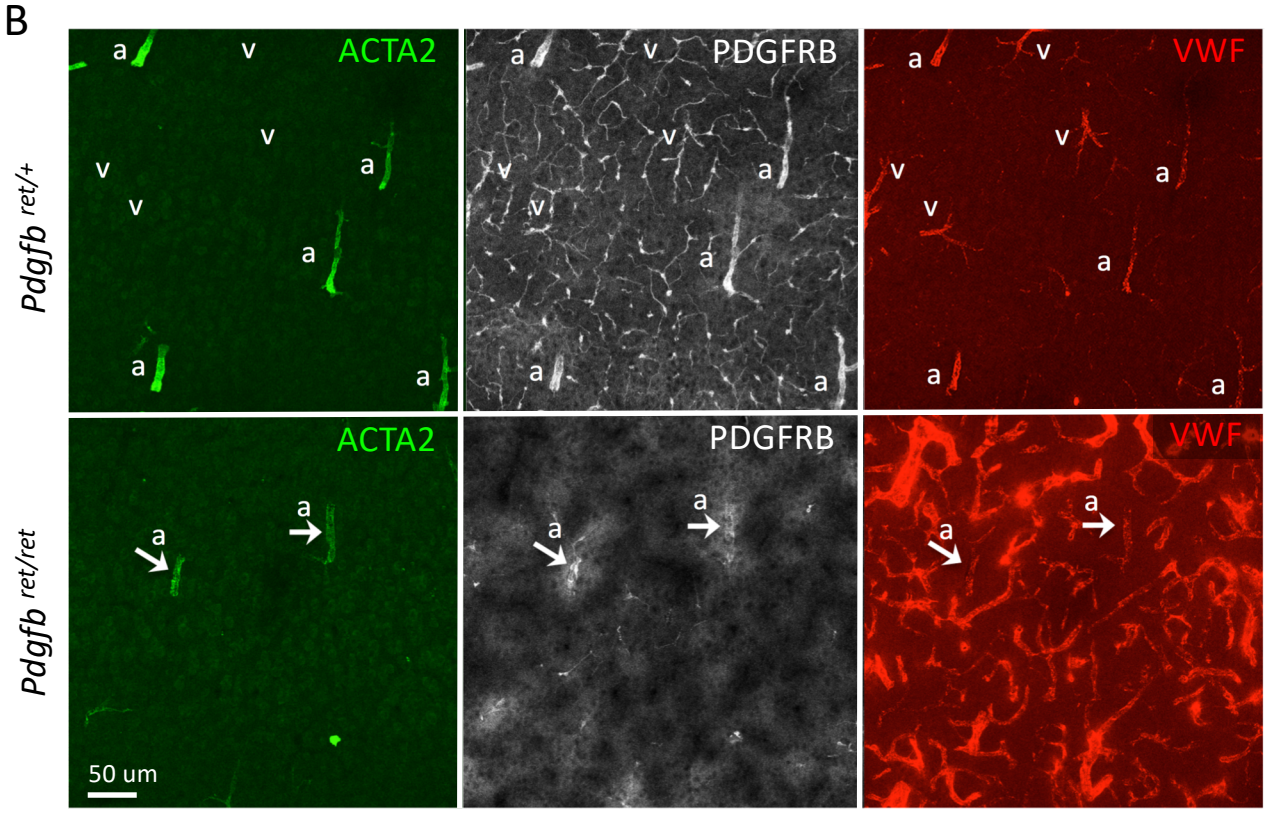
B
Pdgfb ret/+
Pdgfb ret/ret
ACTA2
PDGFRB
VWF
a
v
50 um

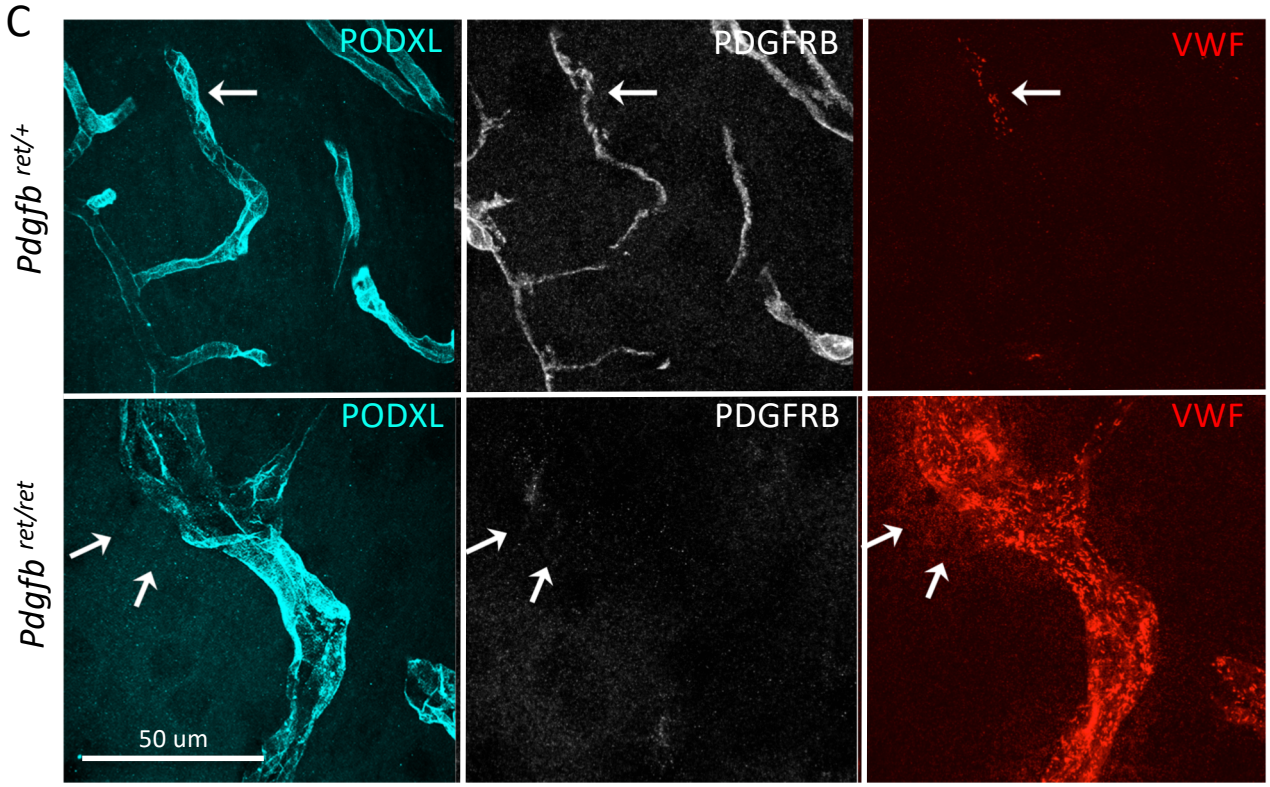
C
Pdgfb ret/+
Pdgfb ret/ret
PODXL
PDGFRB
VWF
50 um

Figure 6

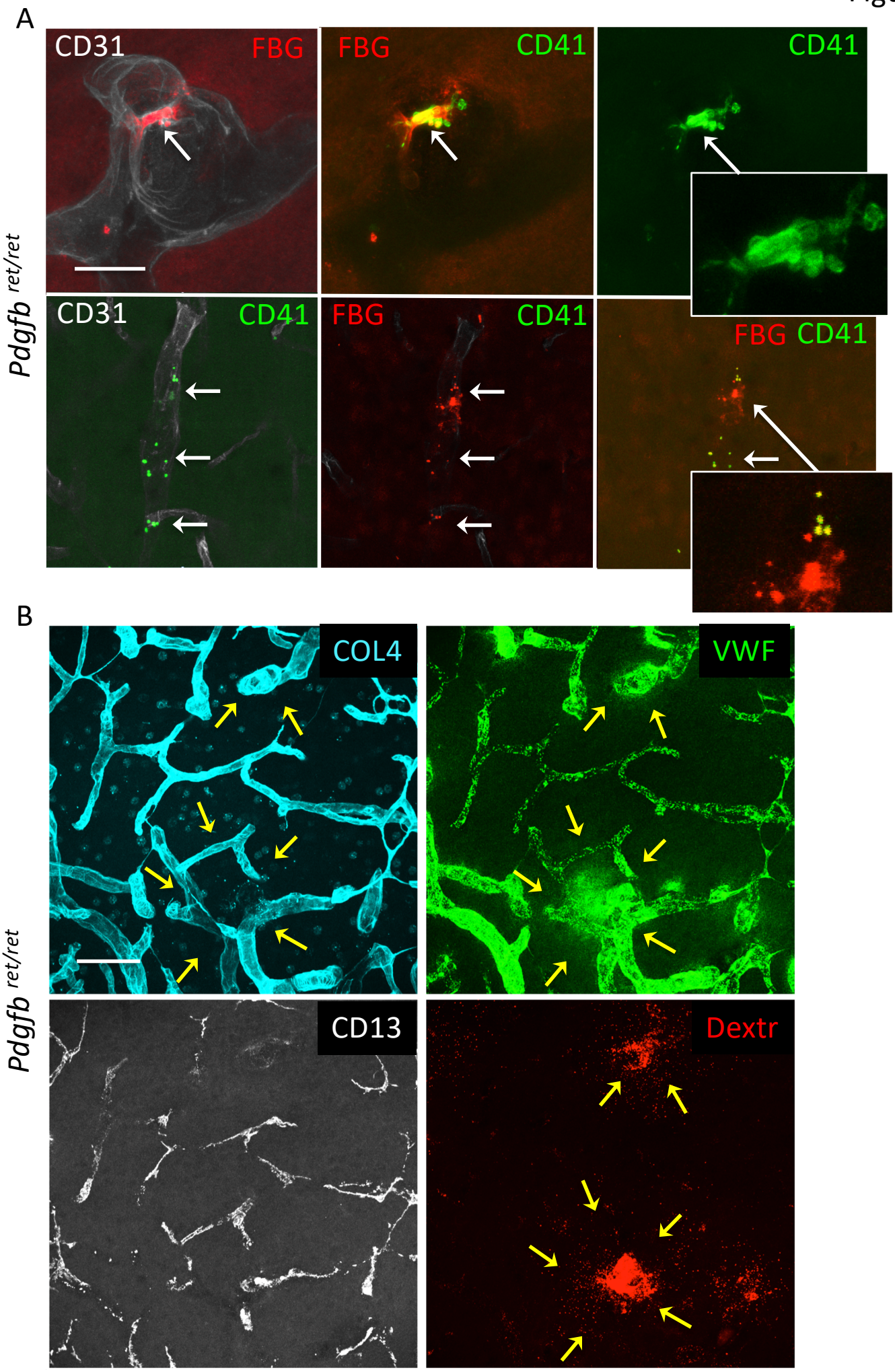
A
CD31
FBG
FBG
CD41
CD41
Pdgfb ret/ret
CD31
CD41
FBG
CD41
FBG CD41
B
COL4
VWF
Pdgfb ret/ret
CD13
Dextr

Figure 7

The COVID-19-pericyte hypothesis

1. Low-risk individuals have a low vascular permeability.

SARS-CoV-2 does not penetrate an intact endothelial barrier.

2. Risk individuals have a leaky endothelial barrier, allowing SARS-CoV-2 to pass the endothelial lining and to reach and infect pericytes.

Dysfunctional endothelial barriers hallmarks inflammation. It is also seen in hypertension, diabetes, ischemic heart disease, stroke, cancer, and other COVID-19 comorbidities.

3. SARS-CoV-2 infection of pericytes may further exacerbate the endothelial barrier dysfunction, promoting increased virus passage across the endothelial lining.

Pericyte injury induces pro-coagulant responses by the endothelium. Immune attack on the SARS-CoV-2-infected pericytes causes microvascular inflammation.

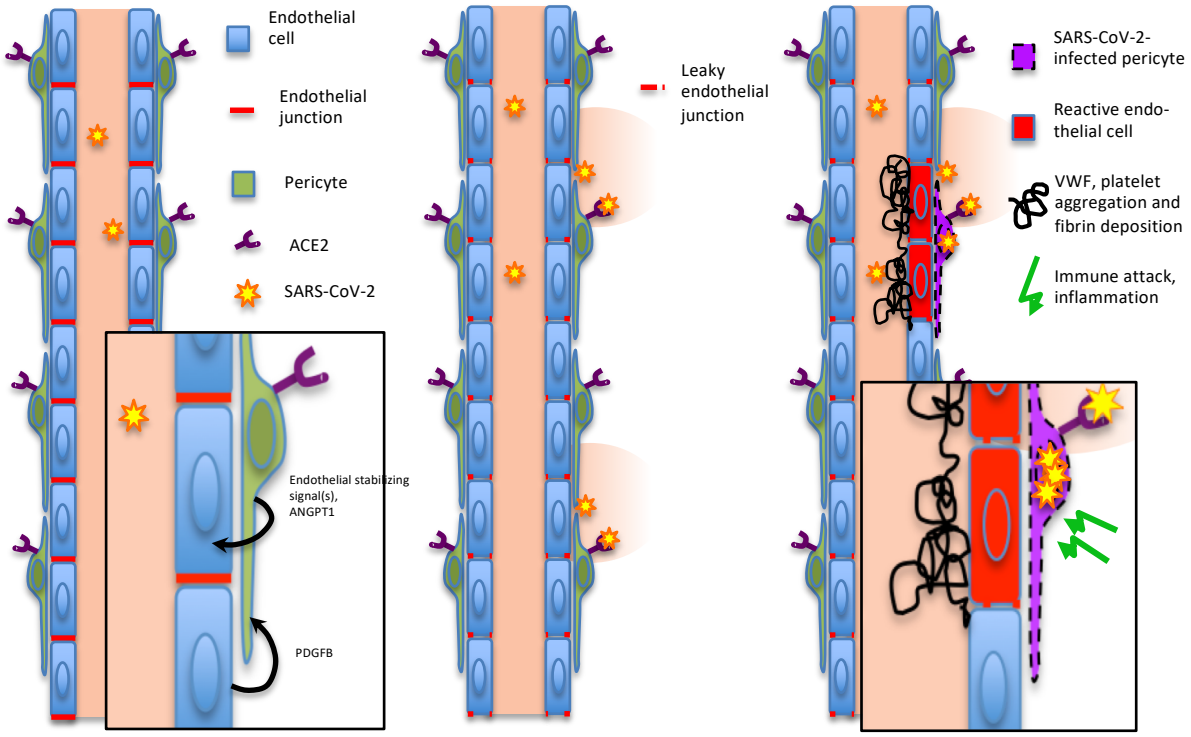

Table 1. Description of a cohort of 20 ICU patients diagnosed with COVID-19.

Patient characteristics in ICU		
Age (years)	63 (40-73)	
Sex (male/female)	18/2	
Patients with riskfactors (n)	17/20 (85%)	
Days with sickness symtoms before ICU admission (days)	10 (2-21)	
Days in ICU (days)	23 (5-37)	
Duration of mechanical ventilation (days)	22 (4-36)	
PFI minimum	11.8 (6-20)	
FiO_2 maximum	0.73 (0.5-1.0)	
PEEP maximum	14 (8-18, 10)	
Patients treated in prone position (n)	17/20 (85%)	
Patients treated with CRRT (n)	10/20 (50%)	
Patients with confirmed tromboembolism (n)	6/20 (30%)	
Secondary infection	12/20 (60%)	
Therapeutic anticoagulation (n)	8/20 (40%)	
Profylactic anticoagulation (n)	15/20 (75%)	
Patients with profylactic ASA (n)	10/20 (50%)	
Patients Systemic Inflammatory Biochemistry		***Reference values***
White cell count max	19.6 (13.6-36.1) x 10 (9)/L	3.5-8.8 x 10 (9)/L
Neutrophile count max	16.7 (3.1-34.1) x 10 (9)/L	1.6-5.9 x 10 (9)/L
Lymfocyte count min	0.5 (0.2-7.2) x 10 (9)/L	1.1-3.5 x 10 (9)/L
IL-1 max	8.3 (5-67) ng/L	<5 ng/L
IL-6 max	670 (83-49544) ng/L	<7 ng/L
TNF-alpha max	36.7 (17.8-67.0) ng/L	<12 ng/L
Ferritin max	2169 (618-9752) µg/L	10-150 µg/L
CRP max (mg/ml)	388 (256-642) mg/L	<3 mg/L
PCT max (µg/L)	9.2 (1.6-306) µg/L	<0.5 µg/L
Patients Systemic Coagulation Biochemistry		***Reference values***
SR	140 (87-140) mm	<10 mm
INR	1.3 (1.0-8.0)	<1.2
APTT	34 (25-119) s	20-30 s
TPK min	199 (19-530) x 10 (9)/L	145-348 x 10 (9)/L
TPK max	487 (89-1171) x 10 (9)/L	145-348 x 10 (9)/L
D-dimer max	8 (2-35) mg/L FEU	<0.5 mg/L FEU
AT III min	0.78 (0.58-1.04) kIE/L	0.8-1.2 kIE/L
Fibrinogen max	9.3 (5.8-15.8) g/L	2-4.2 g/L

Data are presented as median (min-max, range) or numbers (percentage)